Dose calculations for external photon beams in radiotherapy

1999 Phys. Med. Biol. 44 R99

(http://iopscience.iop.org/0031-9155/44/11/201)

Phys. Med. Biol. **44** (1999) R99–R155. Printed in the UK PII: S0031-9155(99)36024-3

TOPICAL REVIEW

Dose calculations for external photon beams in radiotherapy

Anders Ahnesjö† and Maria Mania Aspradakis‡

† Helax AB, Box 1704, Klostergatan 12, 751 47 Uppsala, Sweden
‡ Regional Medical Physics Department, Newcastle General Hospital, Newcastle upon Tyne, NE4 6BE, UK

E-mail: anders.ahnesjo@helax.se and maria-mania.aspradakis@ncl.ac.uk

Received 24 November 1998, in final form 15 July 1999

Abstract. Dose calculation methods for photon beams are reviewed in the context of radiation therapy treatment planning. Following introductory summaries on photon beam characteristics and clinical requirements on dose calculations, calculation methods are described in order of increasing explicitness of particle transport. The simplest are dose ratio factorizations limited to point dose estimates useful for checking other more general, but also more complex, approaches. Some methods incorporate detailed modelling of scatter dose through differentiation of measured data combined with various integration techniques. State-of-the-art methods based on point or pencil kernels, which are derived through Monte Carlo simulations, to characterize secondary particle transport are presented in some detail. Explicit particle transport methods, such as Monte Carlo, are briefly summarized. The extensive literature on beam characterization and handling of treatment head scatter is reviewed in the context of providing phase space data for kernel based and/or direct Monte Carlo dose calculations. Finally, a brief overview of inverse methods for optimization and dose reconstruction is provided.

Contents

1. Introduction

In the early days of radiotherapy, 'dose' was used in a pharmacological sense quantifying the amount of radiation given rather than its physical impact on the irradiated matter. Today, absorbed dose is strictly defined as mean energy imparted (by ionizing radiation) per mass (ICRU 1998), i.e. dose is decoupled from the radiation used to deliver it. Therefore, absorbed dose is the fundamental physical quantity of interest for relating radiation treatment to its outcome. The broad spectrum of events that impart energy to matter implies that direct measurement of dose from its definition is not a trivial task. Calorimeters and ionization chambers can be used to measure dose in absolute terms but are not suitable for *in vivo* dosimetry. Thermoluminescence detectors and diodes, placed on the patient surface or within cavities, are used to check the delivered dose in patients, but they are not suitable for obtaining a map of the dose. Hence, quantification of dose distributions in patients must be based on calculation models, both for treatment planning and in following up the delivered treatment.

When high-energy photon beams were introduced clinically in the 1950s, the only choice available for medical physicists was to develop empirical methods. These methods often restricted treatments to beam set-ups that could be calculated with some confidence. A historical review of treatment techniques with an extensive bibliography of early developments in dose calculations is provided by Fraass (1995). Before access to CT scanning, mapping of patient anatomy had to rely on simple contouring, i.e. dose calculation accuracy was limited to a great extent by the lack of relevant information about the patient. During the early 1970s 'mini-computers' provided enough computational power to enable the development of both CT scanners and computer based treatment planning systems at prices affordable to healthcare providers. These advents boosted the refinement of empirical dose calculation methods to incorporate voxel by voxel considerations of heterogeneous tissues (see reviews of that time, e.g. Purdy and Prasad (1983) or Cunningham (1983)). More recently, imaging modalities such as MRI (nuclear magnetic resonance imaging), SPECT and PET (single photon and positron emission tomography) have greatly increased the possibility of localizing and delineating tumours and nearby organs (Austin-Seymour *et al* 1995, Schad *et al* 1992). In response to greater precision in defining the target volume, a present trend is to explore all available

degrees of freedom in beam delivery in order to increase the target dose and spare normal tissues (Bortfeld *et al* 1997, Brahme 1987, 1995, Chin *et al* 1983, Webb 1997). Increased dose requires increased accuracy, as reviewed in section 3.2. Empirical methods are limited in accuracy and often fail to model generalized beam set-ups. Although the transport equation and the interaction cross sections are well known, no analytical dose calculation algorithms for photon beams have been developed that are general enough to handle radiotherapy geometries with high enough accuracy. Analytical methods might work if a very short chain of events precedes the complete absorption of the particle's energy (or when the photons escape the system of concern). Monte Carlo methods, implemented to mimic the basic processes in a straightforward way, have served many purposes in medical physics (see reviews by Andreo (1991), Rogers and Bielajew (1990) and Mackie (1990)). However, they have not yet become suitable for routine treatment planning of photon beams due to their huge requirement for CPU time. Therefore, a new family of semianalytical dose calculation algorithms based on energy deposition kernels has been developed, as reviewed in detail in section 7.

Traditionally, calculation of dose output and the related irradiation time or the accelerator monitor units has been treated as a separate task, often not integrated into the treatment planning system itself. More recently, attention has been drawn to the importance of characterizing the beam and to fully modelling output and lateral beam variations. The result is a more complete understanding and modelling of dose deposition, thus enabling planning to be carried out for more complicated treatments. Increased requirements on standards for safety and quality assurance during treatment have, on the other hand, emphasized the important role of simple dose calculation methods for independent checks of the output from treatment planning systems.

1.1. The scope of this review

The aim of this work is to review the background, requirements, formalisms and algorithms for photon beam dose modelling in external radiotherapy. Calculation methods for brachytherapy and radiation protection fall outside the scope of this review. The emphasis will be on methods suitable for the implementation and/or check of dose calculations in 3D treatment planning systems. Beginning with introductory sections on the energy deposition processes and clinical requirements for dose calculations, we continue with formalisms for monitor unit normalization followed by several sections on particular dose calculation methods. The methods will be described in order of increasing explicitness of particle transport considerations. The range of modelling starts with empirically oriented techniques (sections 5 and 6) and continues over kernel based methods (section 7) to explicit particle transport methods such as Monte Carlo (section 8). There is, however, no strict division between models based on first-principle particle transport and empirical models. A particular implementation may consist of elements from both groups of models and also apply different monitor unit calibration/normalization formalisms. All models require the incident beam to be characterized to provide basic data as discussed in section 9. Finally, some inverse techniques proposed for beam optimization are reviewed in section 10.

2. Energy deposition in photon beams

2.1. The physical processes

The photons from a treatment machine yield a cascade of interactions, not only in the patient but also in the treatment machine itself before the energy is absorbed as dose (see figure 1).

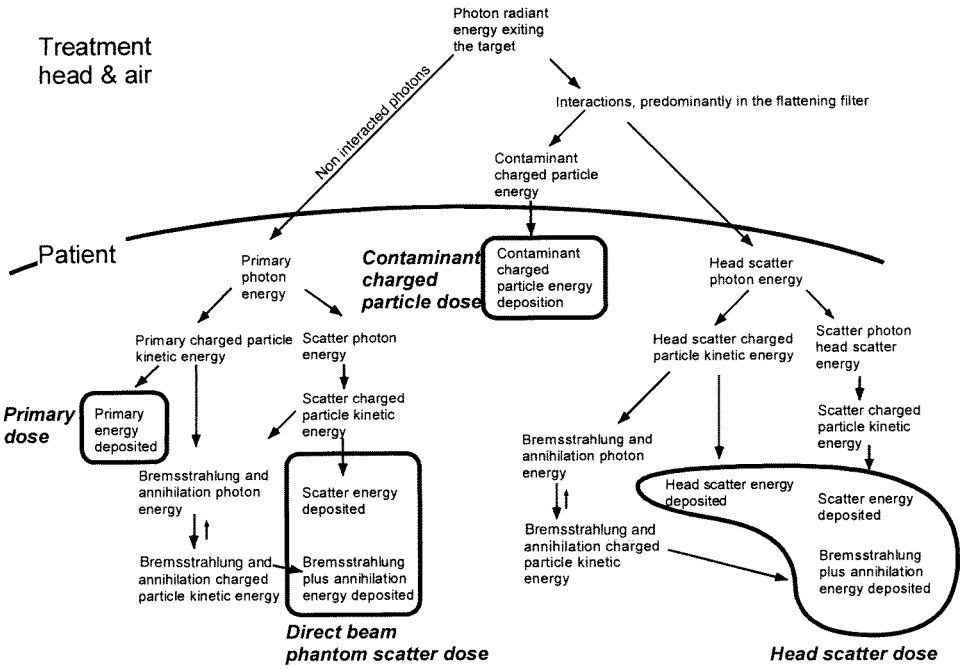

Figure 1. Interaction history of the four dose categories commonly referred to in dose calculations for treatment planning—primary dose, phantom scatter dose, contaminant charged particle dose and head scatter dose.

Following irradiation of the treatment head elements, the beam is scattered adding a secondary photon component to the primary beam. In addition, charged particles released in the treatment machine head and the air column between the head and the irradiated medium contaminate the beam and contribute to the dose in the build-up region. The amount of charged particle contamination is very sensitive to the presence of scattering material. Therefore, dosimetry protocols state that beams should be calibrated at a depth beyond the range of charged particle contamination (IAEA 1987).

Photons are indirectly ionizing particles and do not deposit significant energy themselves. Through interactions with atoms in the patient, the incident photons transfer their energy to electrons and positrons that ionize and excite atoms along particle tracks until their energy is lost. Using the interaction history one can make unambiguous definitions of the various dose categories relevant to beam characterization and dose modelling, as outlined in figure 1. Starting at the source (electron beam target), most photons entering the patient have not been subject to any interactions before entering the patient and will serve as originators of the primary and phantom scatter dose distributions. Particles interacting in the treatment head yield two dose categories: charged particle contamination and head scatter dose. The different order of scatter regarding the head scatter dose is not normally separated. Head scatter dose accounts, depending on beam energy, for approximately 5–15% of the total dose (Ahnesjö 1994).

Since the time of conventional x-rays and ^{60}Co units the importance of charged particle transport has often been overlooked in dose calculations for treatment planning. It has been considered sufficient to assume that the photon energy transferred to such particles was deposited ‘on the spot’ (collision kerma approximation). This has caused confusion, for instance, when ‘primary dose’ has been defined experimentally as ‘zero-area tissue–phantom

ratio' (Mohan and Chui 1985). However, it is convenient to keep the concept of primary dose since its dependence on the primary photon fluence is far more local than the dose mediated by scattered photons (see Bjärngard and Cunningham 1986, Nizin 1993 and Woo *et al* 1990). In ICRU (1987), primary radiation is taken to be the radiation incident on the surface of the phantom and includes photons coming directly from the target as well as radiation scattered from the beam shaping and collimating system. In this review, unless otherwise stated, dose due to radiation that has been scattered within the head of the treatment machine (resulting in head scatter dose) will be considered separately. Reasons for the separation are that head scattering processes are independent of scattering in the patient and results in radiation that differs in energy and direction from the primary beam. In section 9, the literature on head scattered radiation is reviewed in more detail.

2.2. The theorems according to Fano and O'Connor

The dosimetric data used in treatment planning are mainly derived for water. The existence of two important theorems by Fano and O'Connor enables density-scaling of data for water to 'water-like media' with arbitrary densities.

Fano's theorem states that when an object of varying density but constant atomic composition is present in a radiation field with constant fluence of primary particles (photons), then the fluence of secondary particles (electrons) is also constant and independent of the density variations (Fano 1954). This constant fluence of secondary electrons equals the fluence in charged particle equilibrium (CPE) for a given fluence of photons. Consequently the absorbed dose across any area of density variations would be constant. The main assumption in Fano's theorem is that the interaction cross sections per unit mass are independent of the density of a medium of identical atomic composition. Strictly, in order to apply Fano's theorem to external photon beams, one must assume that primary photon attenuation, the stopping power density effect and the release of secondary photons can be neglected. Ignoring photon attenuation essentially means that the mean free paths of primary photons must be much larger than the maximum ranges of the released secondary electrons. This first condition can be fulfilled in clinical beams, with photon energies less than 1–3 MeV and applies to points in an externally irradiated medium which are sufficiently far from boundaries (Harder 1974). Density effects (within the density range of human tissues) are generally small for clinical beams and the production of secondary photons is not problematic as long as their mean free paths are larger than the ranges of secondary electrons. For the above reasons Fano's theorem is an important test of dose calculation algorithms (Nilsson and Knöös 1992). The effect of lateral charged particle disequilibrium is illustrated in figure 2 by the depth dose curves along the central axis in fields of different sizes.

While Fano's theorem applies to situations of charged particle equilibrium, the density scaling theorem by O'Connor relates the dose in two media of different density but equal atomic composition, both irradiated by the same external beam, to each other. According to this theorem, the ratio of the secondary scattered photon fluence to that of primary photon fluence is constant in the two media provided all geometric distances, including field sizes, are scaled inversely to the density (O'Connor 1957). This means that the dose at corresponding points in two media is the same if all dimensions in the irradiation geometries are scaled inversely with density (see figure 3). Both Fano's and O'Connor's theorems rely on a common assumption that the interaction probability (per electron) is independent of density variations between media. The common foundations and relations between these two theorems was analysed by Bjärngard (1987).

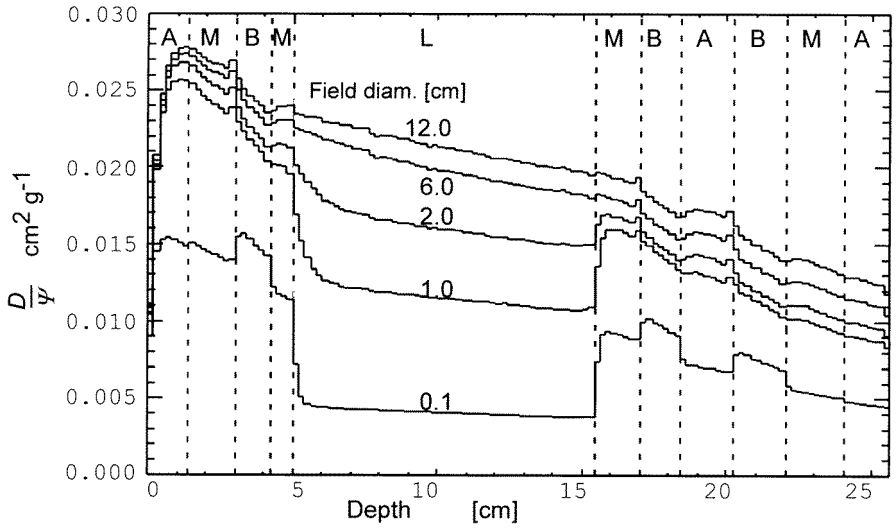

Figure 2. Central axis depth dose curves calculated with the Monte Carlo method for parallel (infinite SSD) 4 MV circular beams of varying diameters (ranging from 0.1 to 12.0 cm) onto a stack of tissue media composed of adipose (A), muscle (M), bone (B) and lung (L) with densities 0.92, 1.04, 1.85 and 0.25 g cm^{-3} respectively. For small fields there is a great difference in dose to different media because of the greatly varying degree of lateral equilibrium of the released charged particles. At larger field sizes the dose is rather constant and declines with depth according to the attenuation of the primary beam. (Adapted from Ahnesjö (1987,1989).)

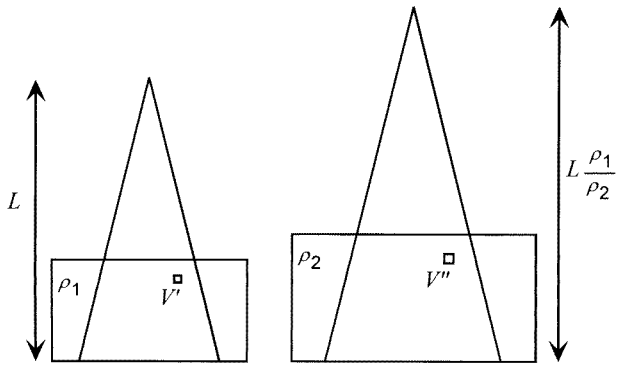

Figure 3. The dose at V' and V'' are equal according to O'Connor's theorem provided that all linear dimensions (including the source to surface distance) are scaled by the phantom density and the number of photons per unit solid angle is equal.

2.3. The reciprocity theorem

For radiation transfer the reciprocity theorem states that *reversing the positions of a point detector and a point isotropic source within an infinite homogeneous medium does not change the amount of radiation detected* (Attix 1986). This theorem dates back to King (1912) who formulated it as a reciprocal relationship between the primary radiation from a point source and a finite volume. Mayneord (1945) extended the theorem to the case where the source and the detector are both extended: *the integral dose throughout any volume whatever*

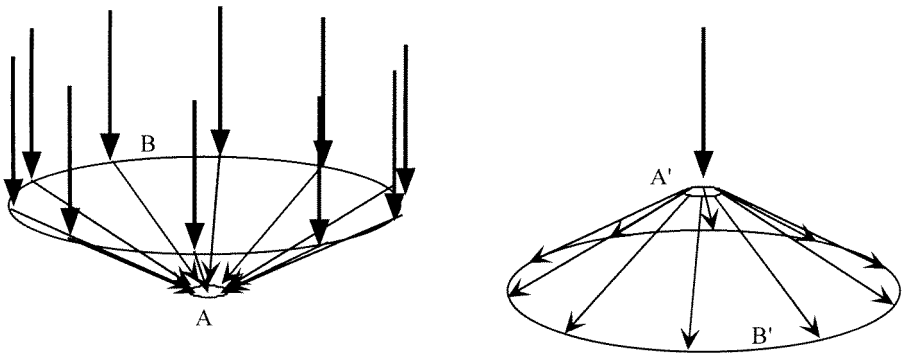

Figure 4. The estimate of dose originating from a large scattering element B to a small element A, as shown to the left, can be made with better scoring statistics by use of a reciprocal geometry as to the right in which A′ is used as the scattering element and B′ as the tally region. The set-up requires a homogeneous medium and rotational symmetric scattering around the primary particle direction for the reciprocity to apply. (Adapted from Hoban *et al* (1994), with permission.)

due to a finite source uniformly filled with radioactive material is equal to the integral dose throughout the original source if the receiver be filled with radiating material of the same uniform density. The implicit approximation in kernel superposition models (see section 7) is that kernels are treated as if the medium were infinite and homogeneous so the theorem applies directly to superposition integrals without requiring further approximations. Although kernels are generally derived assuming an infinite medium, this is not an absolute requirement for superposition calculations. Strictly kernels could be derived at boundary positions and used for superposition calculations (Woo 1994). Kernel reciprocity means that point dose kernels as well as describing the energy deposited around a photon interaction site, also describe the distribution of scattering sites for the particles that mediate energy to a dose deposition point. Due to this reciprocity, comparison between calculated energy spread kernels and measured *iso-line* dose contribution curves was possible (O'Connor and Malone 1989). The application of the theorem in the case of polyenergetic beams where polyenergetic kernels are employed (see section 7.2.1.1) is not exact because of differences in the differential energy fluence spectrum used to define polyenergetic kernels (Papanikolaou *et al* 1993). The reciprocity between photon interaction and dose deposition sites is appropriate for designing geometries for use in experiments or Monte Carlo simulations where signal to noise ratios or statistical uncertainties are of concern (see figure 4).

The reciprocity is also sometimes utilized in radiation transport codes in *adjoint* mode where particles are treated as going backwards from the tally region towards the sources (Difilippo 1998, Wagner *et al* 1994). The technique is best suited to problems where one wants to estimate the response of a small detector exposed to large distributed sources.

2.4. Common experimental quantities

Apart from a summary given as an appendix in ICRU (1976), most of the quantities traditionally used in photon beam characterization lack formal definitions approved by an international body of standardization. Several common quantities have been reviewed in a recent formalism proposal (Dutreix *et al* 1997) with the aim to serve in 'manual' calculations of monitor unit settings. In the present section we give a brief overview of the most commonly used quantities defined for points along the central axis of a photon beam. These are classified into those

quantities that express the depth penetration characteristics of beams, those that attempt to separate scatter dose from primary dose and those that describe the output of the clinical accelerator. The most important of the reviewed quantities are summarized in table 1.

To describe the penetration characteristics, three quantities have been widely used: the percentage depth dose (PDD), the tissue phantom ratio (TPR) and the tissue maximum ratio (TMR). PDD at a point in water is defined as the ratio of absorbed dose at that point to the absorbed dose at the depth of maximum build-up along the central axis. PDD data are impractical for direct reconstruction of dose distributions since they depend on the source to surface distance (SSD). Instead TPR, being independent of SSD, has gained popularity. TPR is defined as the ratio of the total absorbed dose on the central axis at depth to that at a point also on the central axis and at the same distance from the source but with the surface of the phantom moved so that the point is at a specified reference depth (Karzmark *et al* 1965). The TPR was defined to comply with recommendations that x-ray beams should be calibrated at a reference depth in a phantom (ICRU 1963). Another quantity, the tissue maximum ratio (TMR), has been used in some dosimetry systems (Holt *et al* 1970). TMR is renormalized TPR such that the specified reference depth is the depth of maximum dose. The uncertainties due to electron contamination at the depth of dose maximum is a complication, and the use of a reference depth further away from the build-up region, as in the TPR definition, is strictly a better choice for dosimetry systems (Dutreix *et al* 1997).

Early dosimetric systems have tried to separate scatter from primary dose using scatter factors to express the ratio of total to primary dose at a point (ICRU 1973). Tissue air ratio (TAR) was defined as the ratio of the absorbed dose at a given point in a phantom to the absorbed dose at the same point in air, but at the centre of a small volume of phantom material, of mass just large enough to provide electronic equilibrium, at the point of measurement (ICRU 1973, 1976). This definition of TAR (originally known as tumour air ratio by Johns *et al* (1953)), has been a subject of controversy for high-energy beams due to experimental problems in ensuring ideal charged particle equilibrium in air. In a later definition, TAR is relative to the primary

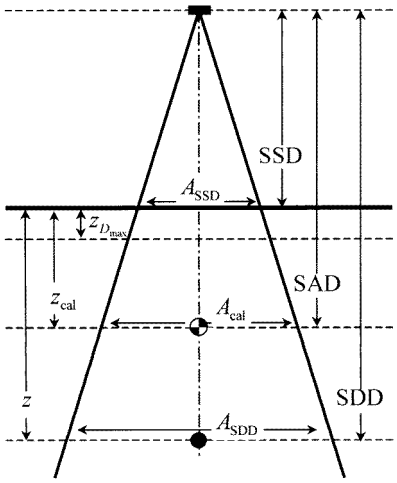

Figure 5. Geometry for specifying some of the quantities given in table 1. The calibration depth z_{cal} is often at isocentre. The acronyms SSD, SAD and SDD read source to surface distance, source to axis distance, and source to detector distance. The generic aperture variable A may, depending on context, represent the entire beam set-up geometry rather than just field size.

Table 1. Some of the most common quantities used in photon beam characterization. The most common abbreviation and symbols in each context have been used (cf figure 5), although some arguments are adapted to follow the nomenclature of this review. For some quantities equivalent concepts have been defined based on the energy fluence formalism adapted from Ahnesjö (1994), Kim *et al* (1998), and section 4.1 (see that section for definitions of variables).

Quantity	Definition	Comment
Percentage depth dose	$\mathrm{PDD}(A_{\mathrm{SSD}};z)=\frac{D(A_{\mathrm{SSD}};z)}{D(A_{\mathrm{SSD}};z_{D_{\max}})}\times 100$	Detector scanned in a fixed SSD beam-phantom system. Aperture size defined at SSD
Tissue phantom ratio	$\mathrm{TPR}(A_{\mathrm{SDD}};z,z_{\mathrm{cal}})=\frac{D(A_{\mathrm{SDD}},\mathrm{SDD};z)}{D(A_{\mathrm{SDD}},\mathrm{SDD};z_{\mathrm{cal}})}$	Phantom moved in a fixed SDD beam-detector system. Aperture size defined at SDD
Tissue air ratio	$\mathrm{TAR}(A_{\mathrm{SDD}};z)=\frac{D(A_{\mathrm{SDD}},\mathrm{SDD};z)}{D_{\text{build-up cap}}(A_{\mathrm{SDD}},\mathrm{SDD})}$	Phantom moved in a fixed SDD beam-detector system. Denominator obtained 'in air' using a build-up cap on the detector
Scatter air ratio	$\mathrm{SAR}(A_{\mathrm{SDD}};z)=\mathrm{TAR}(A_{\mathrm{SDD}};z)-\mathrm{TAR}(A\to 0;z)$	Several procedures proposed to determine $\mathrm{TAR}(A\to 0;z)$
Scatter primary ratio	$\mathrm{SPR}(A_{\mathrm{SDD}};z)=\frac{\mathrm{SAR}(A_{\mathrm{SDD}};z)}{\mathrm{TAR}(A\to 0;z)}$	
Output factor Output factor in water Output ratio in water	$S_{\mathrm{cp}}(A)=\frac{D(A;z_{\mathrm{cal}})}{D(A_{\mathrm{cal}};z_{\mathrm{cal}})}$	Definitions using energy fluence formalism: $S_{\mathrm{cp}}(A)=\frac{D(\Psi_0+\Psi_{\mathrm{hsc}}(A);A;z_{\mathrm{cal}})}{D(\Psi_0+\Psi_{\mathrm{hsc}}(A_{\mathrm{cal}});A_{\mathrm{cal}};z_{\mathrm{cal}})}\frac{(1+b(A_{\mathrm{cal}}))}{(1+b(A))}$
Collimator scatter factor Head scatter factor Output factor in air Mini-phantom output ratio	$S_{\mathrm{c}}(A)=\frac{D_{\text{mini-phantom}}(A,z_{\mathrm{cal}})}{D_{\text{mini-phantom}}(A_{\mathrm{cal}},z_{\mathrm{cal}})}$	$S_{\mathrm{c}}(A)=\frac{\Psi_0+\Psi_{\mathrm{hsc}}(A)}{\Psi_0+\Psi_{\mathrm{hsc}}(A_{\mathrm{cal}})}\frac{(1+b(A_{\mathrm{cal}}))}{(1+b(A))}$
Phantom scatter factor Volume scatter ratio	$S_{\mathrm{p}}(A)=\frac{S_{\mathrm{cp}}(A)}{S_{\mathrm{c}}(A)}$	$S_{\mathrm{p}}(A)=\frac{D(\Psi_0;A;z_{\mathrm{cal}})}{D(\Psi_0;A_{\mathrm{cal}};z_{\mathrm{cal}})}\approx\frac{D(\Psi_0+\Psi_{\mathrm{hsc}}(A_{\max});A;z_{\mathrm{cal}})}{D(\Psi_0+\Psi_{\mathrm{hsc}}(A_{\max});A_{\mathrm{cal}};z_{\mathrm{cal}})}$

dose at the depth of maximum dose build-up, still with constant SDD (BJR 1983 (also in BJR 1996)).

Scatter primary ratio, SPR, is a general name for quantities defined as ratios of scatter versus primary dose at a point. A strict definition for SPR is given by Bjärngard and Petti (1988) where the denominator represents dose originating from primary photons at a depth larger than that of maximum build-up (cf section 4.2). A related quantity is scatter air ratio (SAR) describing the absorbed dose originating from scattered radiation, and is practically derived by subtracting the extrapolated value for zero-area field TAR from finite field TAR (Gupta and Cunningham 1966). The use of extrapolation, however, is ambiguous in strictly representing primary dose (Kijewski *et al* 1986). SAR can be differentiated with respect to field radius to yield differential scatter air ratios (dSAR) (Cunningham 1972, Larson and Prasad 1978, Sontag and Ray 1995). Analogous to SAR, scatter maximum ratios (SMR) (originally called scatter phantom ratios by Khan *et al* (1972)) are calculated by subtracting the zero-area TMR for that depth from the TMR at the same depth and beam radius. In both SAR and SMR the denominator is the primary dose at the depth of maximum build-up. Modelling dose from scattered photons using dSAR or differentiated SPR can be done using various integration techniques (see section 5.2.2). Other commonly used scatter factors are: the backscatter factor (BSF), defined as the SPR at the surface of the phantom on the central axis, and used for low- and medium-energy x-rays, and the peak scatter factor (PSF), used for higher-energy beams and defined at the depth of maximum build-up. Normalized peak scatter factors (NPSF), are PSF renormalized to a reference field size to avoid uncertainties due to scattered photons (Day 1983).

The output from a treatment machine is defined in ICRU 24 (ICRU 1976) as the rate of exposure or dose for a given field related to the same quantity in a reference geometry which usually is the calibration depth and field size. The separation of total output ('output in water') into treatment head scatter ('output in air') and phantom scatter was first done by Holt *et al* (1970). They measured the total output and head scatter factors separately, as they are readily defined, unlike phantom scatter factors which can only be measured with 'field-cut' phantoms with maximum-opened jaws on the machine. Phantom scatter factors, labelled as S_p, are often estimated as the ratio of the total scatter factor S_{cp} to the collimator (head) scatter factor S_c, thereby assuming equal broad beam dose per energy fluence conversion of primary and head scattered photons. (Other common symbols for these factors are OF_{phant}, OF_w and OF_{air} respectively.) This is not strictly true since the diffuse beam of head scattered photons is larger than the well-collimated primary beam, but considering that head scatter is only a fraction of the total the approximation can be used. The various kinds of output factors can be given strict definitions by applying energy fluence formalisms (Ahnesjö 1994, Kim *et al* 1998) (see table 1).

3. Dose calculations for treatment planning

Dose calculation models should serve, within the environment of a treatment planning system, to provide quick and accurate results for all relevant types of treatment field arrangements. The demands on dose calculations are therefore to a large degree context dependent. Important aspects in design of treatment planning systems are not only the accuracy of the results but also the logistics of the data objects, user interface layouts, etc.

3.1. Generality, flexibility and logistics

The general requirements for a treatment planning system were identified early (ICCR 1970) although the technology to realize the goals has only just started to approach the real needs.

Anatomy mapping with CT enabled the modern approach to treatment planning where much of the beam geometry is evaluated by a combination of dose quantification and 'virtual simulation' of a CT study rather than physical simulation with the patient at a simulator (Goitein and Abrams 1983). The 'beam's-eye view concept' (Goitein *et al* 1983) is a classical invention mimicking radiographs to align the beam with identified organs. This concept has now merged with dose calculations as to verify delivered dose by patient dose reconstruction from portal dose distributions (see section 10.2). The use of intensity modulation to optimize beam profiles (see Brahme (1995) for a review) requires that the beam can be modulated to achieve the desired treatment. Use of scanning beams and dynamic multileaf modulation will not affect spectral-dependent beam properties but if attenuating modulators ('compensator filters') are applied, the change in spectral-dependent properties should be accounted for. Hence, the dose model framework must be general enough to include the influence on dose and beam properties from general beam set-ups and modulations, and also be able to follow the particle transport to the portal image plane with adequate details.

Jung *et al* (1997) have studied the clinical workflow and developed design principles to meet logistic demands. As an example it was stated that it should be possible to perform the different tasks in a natural, and as far as possible, arbitrary order. It implies that it could be desirable to know the dose to a single point before a full matrix calculation is done. Most traditional algorithms, that typically take into account only the ray path from the source to the calculation point, can generate dose values at arbitrary points. A modern approach, such as that from convolution/superposition or Monte Carlo, provides the result in a 3D Cartesian grid but calculation efficiency is lost completely if dose has to be delivered point by point. This is of some importance as the number of points where the dose is calculated can be reduced significantly if an optimal set of points is used (Niemierko and Goitein 1990). However, Cartesian grids are sufficient if the grid resolution is high enough (see the paper by van't Veld and Bruinvis (1995) which includes a bibliography). An obvious choice is to have a highly integrated 'single point model' in interactive operation where some accuracy is traded for point dose speed, and a second, more accurate, 'bulk matrix model' which could be allowed to run in batch mode. It is, however, desirable to use a single model in order to simplify clinical verification and quality assurance (although a multimodel system would provide some inherent quality assurance comparing results from the different models). For interactive use, point calculations should be virtually instantaneous and spend a maximum of some tens of seconds in calculating a dose distribution in a patient cross section. The uppermost time limit for an accurate calculation to a bulk volume when no user interaction is required would be 1 h, allowing reasonable patient throughput. Use of optimization based on biological or physical object functions will, however, increase the demand for computational speed since optimization schemes usually use iterative search methods (Gustafsson 1996). For gradient based search methods one also need to know the gradient of the response R with respect to the optimization variable ν:

$$\frac{\partial R}{\partial \nu} = \frac{\partial R}{\partial D}\frac{\partial D}{\partial \nu} \tag{1}$$

i.e. the dose model should provide also the gradient $\partial D/\partial \nu$ besides the dose D. Dose must be recomputed occasionally during the optimization search since the dose response $\partial R/\partial D$ is usually nonlinear and/or constrained. For intensity modulation, ν represents the energy fluence Ψ through a pixel (bixel) of the beam cross section. Commonly, the number of iterations needed in optimization is in the order of 50 to 100 leaving substantially less than a minute for dose calculations alone.

Well defined, standardized data objects will facilitate object oriented approaches using databases to serve treatment planning and dose calculations (NEMA 1998). The current

DICOM standard does not (yet) cover the data set needed for treatment unit characterization. This complicates the modularization of dose calculations into exchangeable modules using different models. Quality assurance on dose and monitor unit settings in treatment planning requires checks of the entire chain from beam characterization measurements to final output calculations. Although, in principle, modern algorithms using kernel superposition or direct Monte Carlo simulations should be superior to more simple, traditional approaches, there is a need for these as independent calculators. Thus, since simpler methods could serve for checking information fed into the treatment planning system as well as results generated by it, space will be devoted in this review to both types of calculations.

3.2. Accuracy

The basis for radiotherapy is that cancer cells are more sensitive to ionizing radiation than normal cells. Important parameters to describe the response are D_{50}, the 50% response dose, and the normalized dose gradient γ (Brahme 1984). For tumour control the D_{50} value increases with tumour size and for normal tissue injury D_{50} decreases with larger irradiated volumes (Källman *et al* 1992b), i.e. the therapeutic window shrinks with increasing tumour size. Values for γ vary from 1.5 to 7, i.e. the uncertainty in delivered dose amplifies between 1.5 to 7 times when viewed as dose related part of the uncertainty in biological response. In an attempt to quantify the actual accuracy needed, Boyer and Schultheiss (1988) studied the influence of dose uncertainty on complication-free tumour control (called 'utility function' in their paper) and concluded that a 1% higher accuracy results in 2% increase of cure. It is not surprising that extensive research has been targeted to develop dose response models suitable for application for optimization of dose distributions in treatment planning (see Brahme (1995) for a review). Major problems are not only the determination of the actual parameters to be used in the models (Ågren-Cronqvist 1995) but also the major foundations of the models which are at present subject to some controversy (Dasu and Denekamp 1999). To improve the state of the art, high accuracy and quality must also be enforced in dose reporting (Overgaard and Bartelink 1995, Dische *et al* 1993). Several general recommendations of dose delivery accuracy have been issued: 5% (ICRU 1976), 3.5% (Mijnheer *et al* 1987), 3% (Brahme 1988). The dosimetric error in absolute dose calibration has been determined by Andreo (1990). Excluding beam monitoring instabilities, the absolute dosimetry uncertainty is stated to be 2.0% for MV photon beams and 1.6% for ^{60}Co. Considering the complexity of the dose delivery process, it is of course difficult to achieve 3% accuracy in practice and it is common to refer to the ICRU 24 (ICRU 1976) value of 5% as the level for corrective action. A conservative approach for setting the limits for dose calculation errors alone is to identify the other errors in the dose delivery chain and vary the dose calculation error to identify the limit where the overall value is seriously affected by the dose calculation error (Ahnesjö 1991). Combining the dosimetry estimates from Andreo (1990) and delivery estimates from Brahme (1988) as a representation of the present technique indicates that dose calculations do not need to be better than 2% (see table 2) with a correction action level at 4%. It is unlikely that revolutionary accuracy improvements in dose delivery will occur in future, although some evolution should be anticipated. Developments in basic dosimetry, detector technology and accelerator stability may cut the errors in dose calibration, beam monitoring and flattening to half their present values. Patient data and beam–patient set-ups are difficult to improve but a reduction to two-thirds of their present values should be possible. Summarizing these expectations, a dose calculation accuracy of 1% will be sufficient as the ultimate future goal.

More specific requirements on commissioning and quality assurance of treatment planning systems have been worked out by Dahlin *et al* (1983), Van Dyk *et al* (1993) and Fraass

Table 2. Determination of accuracy goal in dose calculations. With present delivery and calibration technique 2–3% should be the aim while 1% might be the ultimate accuracy goal.

	Present technique $100 \times \Delta D(1\sigma)/D$	Future development $100 \times \Delta D(1\sigma)/D$
Absorbed dose determination at the calibration point	2.0	1.0
Additional uncertainty for other points	1.1	0.5
Monitor stability	1.0	0.5
Beam flatness	1.5	0.8
Patient data uncertainties	1.5	1.0
Beam and patient set-up	2.5	1.6
Overall excluding dose calculation	**4.1**	**2.4**
Dose calculation	1.0 2.0 3.0 4.0 5.0	0.5 1.0 2.0 3.0 4.0
Resulting overall uncertainty	**4.2 4.6 5.1 5.7 6.5**	**2.4 2.6 3.1 3.8 4.7**

Table 3. Dose and positional accuracy criteria for photon beam dose calculations adapted from Van Dyk *et al* (1993). Percentage figures are specified relative to the calibration value with a conversion to local values (within brackets) for the low-dose region. Positional accuracy values (fourth column) are defined as the distances between measured dose points and the nearest points in a calculated distribution which contain the same dose values (van't Veld 1997, Harms *et al* 1998).

	Central axis (except build-up)	High dose region Low dose gradient	Large dose gradient	Low dose region Low dose gradient
Homogeneous water slab—simple fields	2%	3%	4 mm	3% (∼50%)
Stack of tissue slabs—simple fields	3%	3%	4 mm	3% (∼50%)
Anthropomorphic phantoms—complex beams		4%	4 mm	3% (∼50%)

et al (1998). Based on a general 4% requirement for test of existing systems (and a 2% recommendation as a 'developer's goal') Van Dyk *et al* identified a number of situations which they *a priori* assumed to present variable degrees of difficulty. They also differentiated the accuracy criterion for different dose regions, identifying that 3% local accuracy is almost meaningless in high-gradient regions and low-dose regions (see table 3).

4. Dose per monitor units normalization

Here we shall review three major formalisms for dose per monitor units normalization, one model driven dose-to-energy-fluence formalism, one based on dose-to-kerma relations and one empirically oriented dose-to-dose ratio formalism. This classification is similar to the approach used by Mackie *et al* (1996) in their review, although in this review the formalism aspect will be more thoroughly expressed. By 'formalism' we mean the quantities and their relations needed for a monitor unit calculation, while by 'model' we mean the calculational model used to evaluate the quantities used by the formalism. Hence, a formalism can be viewed as a framework, or 'top level' model, within which different computation models can be implemented.

4.1. Dose-to-energy fluence formalisms

The description here follows the work by Ahnesjö and co-workers (Ahnesjö *et al* 1992a, 1995, Ahnesjö 1994, 1995, Weber *et al* 1996, Åsell 1999). A similar but independent development

has also been presented by Mackie *et al* (1995). The common basic idea utilized is that dose is linear to the amount of radiation the patient is exposed to. The linearity makes it natural to express the dose calculated from 'first principle' models as dose per energy fluence, i.e. a dose calculation 'engine' is supposed to deliver

$$d(x, y, z) = \frac{D(x, y, z|\Psi(A; x, y, z_0))}{\Psi_0} \tag{2}$$

where Ψ_0 is a reference energy fluence level, A is a general aperture variable representing all beam collimating and modulating elements and $D(x, y, z|\Psi(A; x, y, z_0))$ is the absorbed dose at point (x, y, z), given that the lateral energy fluence distribution $\Psi(A; x, y, z_0)$ is defined free in air at a reference distance z_0 from the source. Beam attenuation and divergence are assumed to be intrinsic parts of the dose calculation model and not part of the formalism itself. A natural definition of the reference energy fluence Ψ_0 is the primary (cf figure 1) unscattered energy fluence free in air at the calibration point, normally the isocentre (Ahnesjö 1994). Lateral variations of the primary energy fluence (at z_0) are then related to Ψ_0 by the relative distribution $f(A; x, y, z_0)$ such that $\Psi_{\text{prim}}(A; x, y, z_0) = \Psi_0 f(A; x, y, z_0)$. Adding scattered photons, Ψ_{hsc}, from irradiated parts of the treatment head then yields the total photon energy fluence of the beam as

$$\Psi(A; x, y, z_0) = \Psi_0 \left(f(A; x, y, z_0) + \frac{\Psi_{\text{hsc}}}{\Psi_0}(A; x, y, z_0) \right). \tag{3}$$

Following Ahnesjö *et al* (1992a), the monitor units registered for a given beam are separated in two parts, M_0 and M_b. M_0 is the signal proportional to the forward fluence through the monitor chamber and $M_b = M_b(A)$ is proportional to the fluence of particles backscattered into the monitor from the upper part of the adjustable collimators. The backscatter signal is usually small, i.e. $b(A) = M_b(A)/M_0 \ll 1$. The total energy fluence delivered free in air per monitor unit now follows as

$$\frac{\Psi(A; x, y, z_0)}{M} = \frac{\Psi_0}{M_0}(1 + b(A))^{-1} \left(f(A; x, y, z_0) + \frac{\Psi_{\text{hsc}}}{\Psi_0}(A; x, y, z_0) \right). \tag{4}$$

The link between monitor units and energy fluence is provided by a dose normalization for the calibration geometry of the treatment unit. Combining equations (2) to (4) and simplifying the notation of absorbed dose D yields

$$\frac{D(A; x, y, z)}{M} = \frac{\Psi_0}{M_0}(1 + b(A))^{-1} d(A; x, y, z). \tag{5}$$

By requiring the measured dose, for a calibration field A_{cal} and position $(x_{\text{cal}}, y_{\text{cal}}, z_{\text{cal}})$, to equal the calculated dose for the same conditions, Ψ_0/M_0 follows as the ratio between a measured dose (per monitor unit, corrected for monitor backscatter) and a calculated dose (per energy fluence) for the calibration conditions:

$$\frac{\Psi_0}{M_0} = \frac{[D(A_{\text{cal}}; x_{\text{cal}}, y_{\text{cal}}, z_{\text{cal}})/M]_{\text{Measured}}}{[D(A_{\text{cal}}; x_{\text{cal}}, y_{\text{cal}}, z_{\text{cal}})/\Psi_0]_{\text{Calculated}}}(1 + b(A_{\text{cal}})). \tag{6}$$

Following equations (4) and (5), one can easily identify the models needed for implementation of the formalism. The presence of f and Ψ_{hsc}/Ψ_0 in equation (4) tells us to model the primary energy fluence and head scatter fluence prior to running the dose calculation engine $d(\ldots)$. Collimator backscatter to the monitors requires a model of its own as indicated by $b(A)$. The strength of the formalism is that the required models are exchangeable, i.e. it does not matter if an analytical, kernel or Monte Carlo based model is used to execute the role of $d(\ldots)$ as long as it provides dose per incident energy fluence.

4.2. Dose-to-collision kerma formalisms

An early concept for beam calibration was exposure, which formed the basis for formulation of the tissue-air-ratio method of dose calculation. Through the work of Bjärngard and others, a kerma based formalism has been developed. Displacement effects from charged particle transport, although small except in the build-up region, can be included in order to generalize the approach to be used for higher energies (Hannallah *et al* 1996) but are neglected here for simplicity. Hence, the total dose per primary collision kerma is expressed as

$$\frac{D}{K_c}(A; x, y, z) = 1 + \mathrm{SPR}(A; x, y, z) \tag{7}$$

where SPR is the scatter to primary dose ratio (cf table 1). Collision kerma is proportional to energy fluence through $K_c = (\mu_{en}/\rho)\Psi$, so kerma distributions scales with energy fluence and can be calculated through simple application of attenuation and the inverse square law. Attenuation calculations require a detailed knowledge of the spectrum or careful experimental analysis in narrow beam geometries (cf Bjärngard and Shackford 1994, Bjärngard *et al* 1989, 1990, Bjärngard and Vadash 1995, Karlsson *et al* 1993). The dose per monitor unit follows as

$$\frac{D}{M} = \left[\frac{K_c(A_{cal}; x_{cal}, y_{cal}, z_{cal})}{M}\right]_{\mathrm{Measured}} \left[\frac{K_c(A; x, y, z)}{K_c(A_{cal}; x_{cal}, y_{cal}, z_{cal})}\right]_{\mathrm{Calculated}} \times S_c(A)(1 + \mathrm{SPR}(A; x, y, z)). \tag{8}$$

In this formalism lateral head scatter variations are neglected through the use of position-independent output factors in air. The evaluation for arbitrary fields can be done by various methods and is not dependent on the dose formalism.

4.3. Empirical dose-to-dose ratio formalisms

The aim of empirical dose-to-dose ratio formalisms is to arrive at the dose per monitor unit by using as few and standardized measurements as possible. This is achieved by varying the independent variables one by one and deriving the factor by which the measured dose value changes. In this way, dose is factored into a set of measurable factors ending with a relation to the calibration geometry:

$$\frac{D}{M}(\text{case A}) = \frac{D/M_{\text{case A}}}{D/M_{\text{case B}}} \frac{D/M_{\text{case B}}}{\cdots} \cdots \frac{\cdots}{D/M_{\text{calib.geom.}}} \frac{D}{M}(\text{calib. geom.}). \tag{9}$$

A recent systematic reformulation of the dose-to-dose ratio formalism has been given by Dutreix *et al* (1997). The strength of the formalism lies in that the calculations are simple once the data are available. However, calculations of full spatial distributions are not adequately addressed by this formalism since the factors are rarely spatially separable, i.e.

$$D(x, y, z) \neq D(x_0, y_0, z_0)\frac{D(x)}{D(x_0)}\frac{D(y)}{D(y_0)}\frac{D(z)}{D(z_0)} \tag{10}$$

but this is of minor importance since the formalism is mainly intended for manual spot checks of monitor units calculated by treatment planning systems. The major limitation is that, in principle, complex treatments require separate measurements for each beam set-up.

4.4. Renormalizations

The basic difference between the reviewed formalisms is that different models with different sets of elementary data, such as pencil kernels or tissue phantom ratios, generate dose normalized to different entities. Renormalization of the calculated dose to a common

calibration condition provides a link between different formalisms. As an example, in the implementation of equation (5), the ratio Ψ_0/M_0 is not explicitly required since the formalism may equally well be viewed as a simple renormalization:

$$\frac{D}{M}(A; x, y, z) = \left[\frac{D(A_{\text{cal}}; x_{\text{cal}}, y_{\text{cal}}, z_{\text{cal}})}{M}\right]_{\text{Measured}} \times \left[\frac{d(A : x, y, z)}{d(A_{\text{cal}}; x_{\text{cal}}, y_{\text{cal}}, z_{\text{cal}})}\frac{1 + b(A_{\text{cal}})}{1 + b(A)}\right]_{\text{Calculated}}. \tag{11}$$

Equation (9) already contains the measured dose value for the calibration field and the renormalization is obvious.

5. Heterogeneity corrections and scatter dose calculation based on broad beam data

The classical approach for dose calculations to a heterogeneous geometry is to correct the dose acquired for a similar but homogeneous geometry. More recent methods calculate the dose directly by including effects from heterogeneities directly into the models. The situation for modelling of volume scattering effects is similar; a number of methods estimate scatter variations while newer models make calculations based on particle or energy transport directly. Despite the use of full simulation models in modern treatment planning systems, simple approaches are still needed and will most likely be further refined for independent checks of the treatment planning results. There are numerous reviews on inhomogeneity correction methods in the literature, often categorized according to their ability to regard anatomical information (Purdy and Prasad 1983), their way of modelling primary and scattered photon dose components (Wong and Purdy 1987), or the amount of CT density information they use for 3D scattered photon dose calculations (Mohan *et al* 1981, Purdy *et al* 1987, Wong and Purdy 1990, 1992, Bloch and Altschuler 1995). Here various methods for estimation of heterogeneity corrections will be briefly summarized according to the dimensionality of the density information these apply (Purdy 1992). A section on miscellaneous techniques for scatter dose estimation is also included.

5.1. Corrections and scalings for heterogeneities

It is often practical to describe the influence of a tissue heterogeneity as a perturbation of the dose to a homogeneous phantom exposed to an identical irradiation. Commonly, a correction factor is defined from the dose (dose rate) ratio measured for the heterogeneous geometry versus the homogenous, cf equation (9)

$$\left[\frac{D}{M}(\ldots)\right]_{\text{Heterogeneous object}} = \text{CF}(\ldots)\left[\frac{D}{M}(\ldots)\right]_{\text{Homogeneous water phantom}}. \tag{12}$$

Most methods to estimate the heterogeneity correction factor are based on a direct raytrace from the primary source to the point of interest. More elaborate methods such as the ETAR method also exist.

5.1.1. One-dimensional heterogeneity correction of broad beam dose. Methods that use densities only along primary photon paths and hence approximate the patient as a stack of semi-infinite slabs, different for each ray, are here classified as 1D. This type of correction is also widely applied in 3D treatment planning systems where density information is commonly derived from CT images. As the correction is rather independent of the methods used to arrive at the dose for the homogeneous case, a broad variety, too numerous to be reviewed here, of

combinations of methods have been used to calculate the dose. It must be emphasized that even if all these combinations of methods generate a full 3D dose distribution they cannot be considered a correction for heterogeneities in three dimensions.

5.1.1.1. Primary beam effective pathlength methods (EPL). The idea of EPL methods is to scale the broad beam dose distribution by the factor that the primary energy fluence at the depth of calculation has actually changed as compared with the homogeneous case. Assuming water-like media, the density averaged depth at geometrical depth z is given by

$$z' = \frac{1}{\rho_{\mathrm{w}}} \int_0^z \rho(z'')\,\mathrm{d}z'' \tag{13}$$

where ρ_{w} is the density for water and the 'local' density $\rho(z'')$ is (in most cases) estimated from CT images. In applications, z' either replaces the depth variable directly or is used to construct a correction factor. The following four examples show, in order, the effective attenuation method (where μ_{w} is usually estimated from PDD data), the ratio of TAR, the effective SSD method (Cunningham 1972, Purdy and Prasad 1983), and the isodose shift method (Greene and Stewart 1965, Sundblom 1965), respectively:

$$\begin{aligned}
\mathrm{CF}(z) &= \mathrm{e}^{-\mu_{\mathrm{w}}(z'-z)} \\
&= \mathrm{TAR}(A, z')/\mathrm{TAR}(A, z) \\
&= \frac{\mathrm{PDD}(A, z', \mathrm{SSD})}{\mathrm{PDD}(A, z, \mathrm{SSD})} \left(\frac{\mathrm{SSD} + z'}{\mathrm{SSD} + z}\right)^2 \\
&= \frac{\mathrm{PDD}(A, z - n(z - z'), \mathrm{SDD})}{\mathrm{PDD}(A, z, \mathrm{SDD})}
\end{aligned} \tag{14}$$

where n is an empirical constant. EPL methods model the primary dose variation satisfactorily, except for situations of severe charge particle disequilibrium such as for higher beam energies in the lung. However, the amount of scattered radiation reaching the calculation point depends on both position of the inhomogeneity as well as on its size. Therefore, when calculating dose far away from an inhomogeneity, EPL methods give results with acceptable errors but for a complex heterogeneous medium and for dose calculations within or in the near vicinity of an inhomogeneity, EPL methods yield large errors (Sontag and Cunningham 1977).

5.1.1.2. Power-law (Batho) method. This method was suggested by Batho (1964) as an *empirical* correction to account for both primary beam attenuation and scatter changes within water and below a single slab of lung material with density relative to water of 0.35. Sontag and Cunningham (1977) generalized the method to handle arbitrary densities and non-water-like materials. Later, Webb and Fox (1980) and Cassell *et al* (1981) went further to allow for multiple regions of slab-like materials. Finally, El-Khatib and Battista (1984) and Thomas (1991) showed that the correction factor should be based on build-up depth-shifted TMRs instead of the initially proposed TARs such that

$$\mathrm{CF}(z) = \frac{(\mu_{\mathrm{en}}/\rho)_N}{(\mu_{\mathrm{en}}/\rho)_{\mathrm{w}}} \prod_{m=1}^{N} (\mathrm{TMR}(z - z_m + z_{\mathrm{bu}}))^{(\mu_m - \mu_{m-1})/\mu_{\mathrm{w}}} \tag{15}$$

where μ_m and μ_{w} are the linear attenuation coefficients of the material in layer m and water respectively, $(\mu_{\mathrm{en}}/\rho)_N$ is the mass energy absorption coefficient of the material in layer N, z_{bu} is the buildup depth and z_m is the distance along the beam from the surface to the layer m in the phantom. Wong and Henkelman (1982) have demonstrated the fundamental limitations of the original and generalized Batho method through a theoretical analysis carried out on

the calculation of primary and first scatter photon dose and supported their findings with experimental verifications. According to these, the generalized power-law method provides an acceptable approximation below a single inhomogeneous layer with an extent larger than that of the field size and electron density less than that of tissue. In the extreme situation of a large inhomogeneity with electron density greater than tissue and large field sizes, the method has been proved to be inadequate with errors up to 10%. If the electron density (relative to water) of the inhomogeneous layer is greater than unity, the power-law method overestimates the dose. For the calculation of dose within an inhomogeneous layer, generalized corrections perform well when the relative electron density of the inhomogeneity is less than unity, but results become progressively worse for denser layers and larger field sizes. It is also clear that the method is limited by the requirement of lateral charged particle equilibrium, i.e. small fields of high-energy beams in lung may cause very large errors (El-Khatib and Battista 1984, Thomas 1991).

5.1.1.3. Corrections based on 1D convolutions with exponentials. Several authors have constructed heterogeneity corrections based on essentially the following statement: 'particles released from primary interactions in a (thin) slab deposit their energy proportional to exponential attenuation functions of the radiological distance from that slab'. Convolving the attenuated deposition with the sources of primary interactions Iwasaki (1985, 1990), Petti *et al* (1987) and van de Geijn (1987) demonstrated results for a photon beam entering a phantom of media layered across the beam direction. Lateral effects were commonly included by using data dependent on field size, typically scaled from water data using O'Connor's theorem. In the work by van de Geijn *et al* , it was shown that their method is accurate within 1–2% for all energies examined regardless of the field size. At 10 MV and higher energies the performance on the central axis was considered quite acceptable with errors increasing with decreasing field sizes. More recently, Ahnesjö *et al* (1992b) have derived a simple formula for correction of dose due to scattered photons (equation (21) in their paper). Combined with an effective pathlength scaling of the primary dose, their method proved to yield a total dose accuracy on the 2–4% level except for situations of lateral charged particle disequilibrium (small fields of high-energy beams in low-density regions) where larger errors occurred.

5.1.2. The equivalent tissue air ratio method (ETAR). The equivalent tissue air ratio method (ETAR) (Sontag and Cunningham 1978a, b) was developed as a method to be directly implemented on computers available at the time of its introduction. Despite its limitations, ETAR was widely implemented in commercial treatment planning systems during the 1980s and is still in use in many clinics. It can be considered as the first practical method for computerized treatment planning using CT data. Using the density scaling theorem (O'Connor 1957), the TAR in a field of radius A_r at depth z in a medium of density ρ relative to water, is equal to $\mathrm{TAR}(\rho A_r; \rho z)$; the tissue air ratio in a unit density medium for field size ρA_r and depth ρz. The ETAR correction factor is formally defined as

$$\mathrm{CF} = \mathrm{TAR}(\rho A_r; \rho z)/\mathrm{TAR}(A_r; z) \tag{16}$$

which is strictly valid only for homogeneous, non-unit-density water-like media. The application to heterogeneous geometries is carried out by replacing ρA_r by $\tilde{\rho}_r A_r$ and ρz by $\tilde{\rho}_z z$ where $\tilde{\rho}_r$ and $\tilde{\rho}_z$ are 'effective' densities, estimated by 'practical', approximate algorithms. The method devised by Sontag and Cunningham (1978b) derives $\tilde{\rho}_z$ by averaging CT values along primary photon ray paths (similar to the effective pathlength methods). For $\tilde{\rho}_r$ they stated that there must exist a set of weights such that the mean density weighted over the entire irradiated volume equals $\tilde{\rho}_r$. Such weights should consider the conditions of irradiation, the

irradiated medium and the location of the calculation point, a procedure that in itself would require extensive modelling. An approximate estimation of weighting factors was proposed in the appendix of the original paper (Sontag and Cunningham 1978b): all CT slices were 'coalesced' to form an effective slice at the plane of calculation; thus reducing the 3D volume summation to a 2D summation since the primarily goal at the time was to calculate dose to a single slice. The approximation is not easily interpretable for error estimates. In any case, the ETAR method represented a major improvement over the state of the art at the time of its introduction and pioneered the use of CT distributions in treatment planning.

Due to its widespread implementations several workers have attempted to improve the performance of ETAR in various aspects. Woo *et al* (1990) aimed to improve modelling of different dose categories by using data from Monte Carlo simulations and pointed out analogies of their extended concept with the kernel methods. Redpath and Thwaites (1991) generalized the original concepts to account for beam modulation and derive 3D dose distributions. Yu and Wong (1993) recasted the basic formulations and applied the convolution theorem to design a calculation approach orders of magnitude faster than the original ETAR.

5.2. Scatter dose estimation

Calculation of the scatter dose as a function of field size and shape is a long-standing issue in photon beam calculations. Two common approaches are reviewed here, one that circumvents explicit integrations by using data measured for simple square or circular fields of 'equivalent' sizes, and one that employs parametrized scatter dose representations to facilitate integrations over the field shape.

5.2.1. Equivalent field sizes. The simplest way to estimate the total dose at a point in a homogeneously irradiated phantom from a beam with non-standard (rectangular or irregular) shape is to use measured data for an 'equivalent field', i.e. a square or circular field of such size that gives the same scatter dose as the non-standard field (Johns *et al* 1949, Day 1950, 1978). Based on a linearization of the scatter contribution, Bjärngard and Siddon (1982) proved that the radius of an equivalent circular field for a square field with side s is given by

$$r = 2s \ln(1 + \sqrt{2})/\pi = 0.5611s \tag{17}$$

which explained the earlier work of Day (1972, 1978) who semiempirically used this relation and derived tables of equivalent fields (independent of energy and depth) that are still successfully used (BJR 1996). Investigations using measured data (Tatcher and Bjärngard 1993) and Monte Carlo calculated pencil beam kernels (Ahnesjö *et al* 1992b) have further confirmed the work by Bjärngard and Siddon and supported the use of the method as a convenient estimate of depth dose distributions in simple geometries. In an analogous manner, the equivalent square s of a rectangular field of dimensions $L \times W$ is derived from

$$s = \frac{2LW}{L + W} Y(L/W) \tag{18}$$

where Y is defined as the elongation factor. Values of Y are tabulated by Bjärngard and Siddon (1982). Equation (18) without the elongation correction factor has been known as the area-to-perimeter ratio (4A/P method) and was first used empirically by Sterling *et al* (1964) and later examined by others (Patomaki 1968, Worthley 1966, Wrede 1972). Essentially, the 4A/P method equates the central axis dose of any field with that of a circular field of the same area, which can lead to serious errors (Day and Aird 1996).

5.2.2. Scatter dose representation and integration techniques. The representation of scatter dose and related integration techniques has been addressed by many authors. Such scatter functions can be derived from measured data, analytical calculations or Monte Carlo calculations. The most well known scatter representation is scatter air ratios (SAR) and differential scatter air ratios (dSAR) as defined by Cunningham (1972) (cf section 2.4). Recent work by Sontag and Ray (1995) introduces the calculation of dSAR (from measured data and analytically) that correspond to different orders of photon scattering. An alternative representation of scatter dose is given using scatter phantom ratios and in particular scatter primary ratios (SPR). Bjärngard and Petti (1988) and later Bjärngard and Vadash (1995) have showed semiempirically that SPR at depth z on the central axis (excluding the buildup region) of homogeneous fields with square side s could be approximated by

$$\mathrm{SPR} = \frac{asz}{ws + z} \tag{19}$$

where a and w are estimated from a limited set of measurements. Furthermore, Bjärngard and Vadash (1995) showed that a is related to the probability that scattered photons are produced, and w to their directional distribution. Storchi and van Gasteren (1996) and Sätherberg *et al* (1996) have also developed parametrizations, as functions of beam quality index, for the scatter to primary dose ratios at 10 cm depth in water phantoms. The parametric representations of scatter data, combined with equivalent field size approaches have proven to be of great value for quality control of both measured data and monitor unit calculations from treatment planning systems (Bjärngard *et al* 1997). Furthermore, pencil kernel data can be derived from radial differentiation of scatter functions thus forming a bridge between traditional empirical methods and modern Monte Carlo methods for kernel determination (Ceberg *et al* 1996).

Dose for general field shapes can be derived through integration over the field aperture of appropriately differentiated scatter data or representations such as equation (19) (cf section 7.3 on pencil kernel methods). An early integration method that has been widely applied is the approximate summation technique according to Clarkson (1941) and implemented into a widespread computer program by Cunningham *et al* (1972). Here the field around the point of calculation is separated into a number of angular segments and the scatter contribution from each segment is estimated by use of measured data. The Clarkson method works well for simple field shapes but runs into methodological problems for complicated field shapes. Siddon *et al* (1985) developed a far more general method based on triangular decomposition of the surface integral. This method works for any field shape that can be described by a set of closed polygons (where blocks are described by polygons of opposite direction) and can also utlilize parametrizations such as equation (19).

6. Implicit modelling of scattered particle transport

Implicit modelling of particle transport through scaling operations is less computationally intense than a full, explicit modelling of particle interaction and transport. Hence, implicit modelling methods have been extensively studied as illustrated in the following with three different approaches, namely the differential scatter air ratio, the delta volume method and the kernel based methods. The first two approaches have never been widely applied but deserve attention since they highlight some aspects common to the modern kernel based models. Kernel based methods, finally, are treated separately in section 7.

6.1. The differential scatter air ratio model (DSAR)

The first method to address the 3D problem of dose to heterogeneous phantoms by scaling first- and higher-order scatter as first scatter was the differential scatter air ratio method as proposed by Beaudoin (1968). Cunningham (1972) later published how scatter air ratios (SAR) can be derived from tissue air ratios (TAR), and further how the former can be differentiated to give differential scatter air ratios (dSAR). These describe contributions to dose at a point in water from photons scattered in surrounding volume elements as a function of the distance to that point. Scatter dose contributions $(\mathrm{dSAR}/\mathrm{d}V)_{\mathrm{medium}}$ at point $\boldsymbol{r}$ in an inhomogeneous medium from a volume element at $\boldsymbol{r}'$ are expressed in the DSAR method as

$$\left(\frac{\mathrm{dSAR}}{\mathrm{d}V}\right)_{\mathrm{medium}} = \left(\frac{\mathrm{dSAR}}{\mathrm{d}V}\right)_{\mathrm{water}} \rho_e(\boldsymbol{r}')\, f_1(\boldsymbol{r}')\, f_2(\boldsymbol{r}, \boldsymbol{r}') \tag{20}$$

where $\rho_e(\boldsymbol{r}')$ is the electron density relative to water at the scattering site, f_1 is a factor describing the attenuation of the beam relative to water between source and volume element ΔV and f_2 is a factor describing the attenuation of secondary photon fluence relative to water along the path between ΔV and the dose calculation point. Factors f_1 and f_2 can be derived from the Klein–Nishina cross sections and the relative electron density at the dose calculation point and along the assumed rectilinear path of scatter transport respectively. The approach is differentiated enough to model beam modifiers and irregular fields and an accuracy of $\pm 2\%$ in simple heterogeneous geometries has been reported (Cunningham and Beaudoin 1973, Larson and Prasad 1978).

Although DSAR methods employ 3D scatter ray-trace procedures and measured SAR to represent the overall scattering strength of a voxel, it has been shown to be inaccurate when modelling the irradiation of a heterogeneous phantom with large field sizes and at low energies (Sontag 1979). This has been interpreted as that a first scatter ray-trace model is incompatible with the use of SAR data which implicitly contain contributions from multiply scattered photons (Cunningham 1972). The original DSAR model has been examined only for ^{60}Co beam. Implementation at higher energies would suffer from the lack of electron transport modelling due to difficulties in representing primary and scattered photon contributions from measured (extrapolated) zero area TAR and SAR respectively. Redpath (1995) described a simplified implementation of the DSAR philosophy where electron transport is ignored and scatter dose is calculated in an approximate manner by assigning factor f_2 of equation (20) equal to the relative electron density at the point of interaction (similarly to simplified FFT kernel based convolution methods; cf section 7.2.2.2). Another limitation of the DSAR method is that backscatter is not modelled due to the difficulty in deriving explicit backscatter differential scatter air ratios from TAR (Wong and Purdy 1990).

6.2. The delta volume model

Although some earlier work might have been labelled as the delta volume method due to the use of differential SAR from small volume elements, it is the work by Wong and Henkelman which is generally recognized as the delta volume method (Wong and Henkelman 1983, Wong *et al* 1984). Dose at a point in a heterogeneous medium is calculated as a sum of the primary dose, an augmented first-scatter dose component and an approximate residual multiple- scatter component. Relative primary dose is obtained similarly to the DSAR method from the knowledge of the primary intensity in air and the density along the path of the primary photons. The augmented first-scatter component includes the part of the second-order scatter that was considered to be effectively transported as first scatter (scattering angles less than 45°). Both these components were pre-calculated

as a kernel using cross-sectional data and scaled to actual geometries by explicit ray tracing. The residual multiple-scatter dose component is modelled in a way that resembles ETAR scaling of SAR with density. In this term, empirical data representing the dose perturbation from introduction of a small void in an otherwise homogeneous water phantom are used.

The physics behind the scatter modelling in the delta volume method has been well examined and justified for ^{60}Co beams through investigations of the scatter dose properties (Wong *et al* 1981a, b). The method succeeds in satisfying the two constraints identified by Wong and Henkelman (to correctly calculate the dose to (a) water with a small void and (b) homogeneous non-water medium), it approximately calculates the multiple-scatter dose component, and since it is using augmented scatter values and multiple-scatter perturbation values from each scattering element it directly accounts for backscatter. The computational burden, absence of electron transport modelling, reliance on experimentally cumbersome data and lack of development for higher beam energies have made the method of less interest for implementation into commercial treatment planning systems.

7. Kernel based models (convolution/superposition)

Kernel based convolution/superposition models are a family of models with roots in the imaging world. Analogous to image formation, the dose deposition is viewed as a superposition of appropriately weighted responses (kernels) to point irradiations. Under conditions where the kernels are spatially invariant, the superpositions can be efficiently evaluated by means of convolutions. The kernels, representing the energy transport and dose deposition of secondary particles stemming from a point irradiation, are not usually accessible through measurements but are very simple to calculate by use of Monte Carlo particle transport codes. The earliest record of point kernels in dosimetry known to the authors is by Loevinger (1950, 1956). The buildup region from a betatron photon beam depth dose was explained by a one-dimensional forward scatter function approach by Johns *et al* (1949). Later Roesch (1958) introduced kerma (which he called 'kerm') and defined an 'influence function' that distributes the kerma energy at a point into absorbed dose at surrounding points. Dutreix *et al* (1965) used buildup curves for various narrow circular fields to determine the approximate shape of the Roesch influence function. Brahme (1977) used an equivalent concept to calculate restricted mass energy absorption coefficients for use in dosimetry. Dean (1980) used point kernels for 1.25 MeV gamma rays together with experimental data from LiF thermoluminescent dosimeters, for the calculation of the relative amount of scatter dose. Schoknecht (1971) and Ulmer (1982) used pencil kernels in a convolution process to demonstrate calculations of dose distributions.

The potential for kernel based models in treatment planning did not attract much interest until 1984 when the concept was brought forward by several independent investigators (Ahnesjö 1984, Boyer and Mok 1984, Chui and Mohan1984, Mackie and Scrimger 1984) and later worked out in more detail (Boyer and Mok 1985, Mackie *et al* 1985, Mohan *et al* 1986, Ahnesjö *et al* 1987). Although the formulation of the method in its basic form is simple and appealing, the demands on computer time combined with the need for modelling of various second-order beam characteristic effects have delayed its clinical implementation until recently. Kernel models can explicitly handle the degree of freedom posed by modern treatment machines without any major approximations and it is therefore generally anticipated that they will be the workhorse for conformal therapy applications (Webb 1993). In the following sections we shall review the kernel superposition approach more in detail.

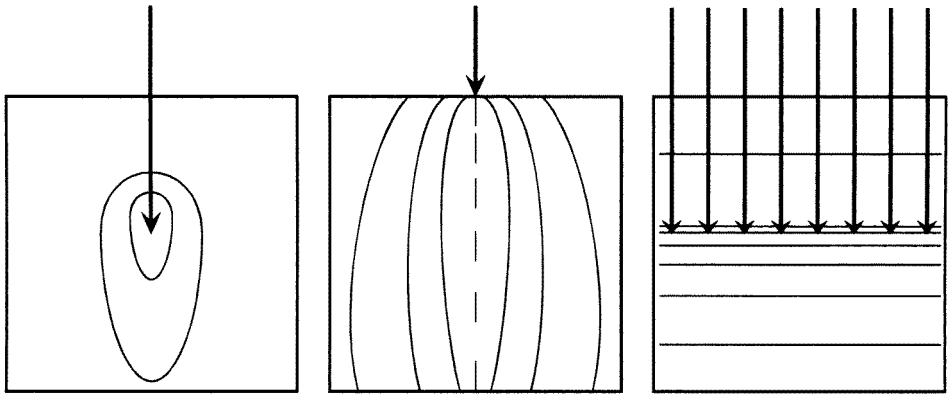

Figure 6. Irradiation geometries for point kernels (left), pencil kernels (centre) and planar kernels (right). Isodose curves are shown as full curves.

7.1. Energy deposition kernels

Photons can travel large distances unaffected and the energy and direction of a primary photon is therefore independent of where it interacts. The energy deposition by secondary particles around a primary photon interaction site is, in homogeneous media, independent of the location of the site and can be described by a kernel. Energy deposition kernels (EDK) are defined as the distribution of energy imparted to volume elements (per unit volume) in a medium, commonly water, due to an elemental photon beam incident at the origin of coordinates of the kernel. Energy deposition kernels are categorized according to the geometry of the elemental beam that delivers the incident energy. Essentially three different kernel geometries have been defined (see figure 6). The kernel describing the pattern of energy deposited in an infinite medium around a primary photon interaction site is known as a *point kernel* (called dose spread array by Mackie *et al* (1985), differential pencil beam by Mohan *et al* (1986) and point spread function by Ahnesjö *et al* (1987)). A *pencil kernel* describes the energy deposition in a semi-infinite medium from a point monodirectional beam and a *planar kernel* describes the forward and backward energy spread from primary interactions located in a plane, laterally oriented in an infinite broad beam. Sometimes also a fourth type, a *rotated* kernel, describing the deposition of energy due to convergent irradiation of a rotationally symmetrical phantom, has been used for inverse calculations (see section 10.1).

There are several possibilities for normalization of kernels, dependent on the formulation of the dose equation they will be part of. The common approach is to normalize to the radiant energy to be distributed by the kernel, i.e.

$$h(\boldsymbol{r}) = \frac{\mathrm{d}\varepsilon}{R\,\mathrm{d}V} \Rightarrow \iiint_{\infty} h(\boldsymbol{r})\,\mathrm{d}V \equiv 1 \tag{21}$$

where $\mathrm{d}\varepsilon$ is the mean energy imparted in the volume element $\mathrm{d}V$ due to the interactions the radiant energy R undergoes before it is deposited as dose. Alternative approaches have been used by Boyer (1988) who normalized the kernel towards the fluence of the primary particles, and by Mohan *et al* (1986) who normalized the kernel to the number of interacting primary particles. Kernels are often separated into different dose categories according to the scattering history of the depositing particle (cf figure 1). Separating a point kernel into two parts, one for

the primary dose (h_p), and one for the phantom scatter dose (h_s), the kernel integral is closely related to the energy absorption coefficients as pointed out by Mackie *et al* (1988) and Boyer (1988). Using the normalization in equation (21), it follows that

$$\iiint_{\infty} h_p(\boldsymbol{r})\,\mathrm{d}V = \frac{\mu_{en}}{\mu} \qquad \iiint_{\infty} h_s(\boldsymbol{r})\,\mathrm{d}V = \frac{\mu - \mu_{en}}{\mu} \tag{22}$$

where μ_{en} is the linear energy absorption coefficient and μ the linear attenuation coefficient. This comprises a useful check for verifying the generation of primary and scatter kernels and is also of importance for constructing corrections for beam quality variations.

The complexity of coupled electron/positron–photon transport limits the possibilities for analytical methods for calculating kernels. The standard method for calculation of kernels is therefore direct Monte Carlo simulations of the particle transport (Ahnesjö *et al* 1987, Mackie *et al* 1988, Mohan *et al* 1986). This is straightforward, although somewhat demanding on CPU time. Analytical *modelling* of the primary dose kernel has been done by Wang *et al* (1995) using Gaussian multiple scatter theory. In photon transport, the first scatter kerma kernel is particularly simple to derive and has been utilized in convolution schemes proposed by Boyer and Mok (1985) and by Nilsson and Knöös (1992). Both groups also devised approximate methods for derivation of the residual, multiple scatter kernels. Boyer and Mok modelled the kernel for multiple scattered photons assuming that they are isotropically distributed around a first scatter interaction site. Nilsson and Knöös also proceeded from the first scatter kernel and used a buildup factor to model the multiple scatter contribution. Analytical *fitting* to simplify the use of kernels has been done for point kernels (Ahnesjö 1989, Ahnesjö and Mackie 1987) and for pencil kernels by Ahnesjö *et al* (1992b). The approach used by Ahnesjö for polyenergetic point kernels was to model the kernel as mediated by rectilinearly transported particles with exponential attenuation and inverse square divergence according to

$$h(\boldsymbol{r}) = \frac{A_\theta \mathrm{e}^{-a_\theta} + B_\theta \mathrm{e}^{-b_\theta}}{r^2} \tag{23}$$

where A_θ, a_θ, B_θ and b_θ are fitting parameters depending on the scattering angle θ. The separation of primary and scatter was such that the first term mainly describes the primary and the second term the scatter dose fraction.

Energy deposition distributions must, when calculated by Monte Carlo, be scored in finite voxels. The larger the voxels the better the statistical accuracy and therefore all workers have utilized the rotational symmetry of spherical or cylindrical binning to increase the scoring volume of distant voxels. Applications of kernels are facilitated through binning these in a problem-specific coordinate system. For example, Fourier transform convolution requires a Cartesian binning, pencil kernels are most natural to use in cylindrical coordinates, and radial scaling of point kernels for heterogeneities is best carried out using the radial bins of a spherical coordinate system. Scaling and change of the coordinate system requires rebinning or interpolation between kernel values scored in neighbouring bins. In low-gradient regions this is trivial, but care must be taken close to the primary interaction site since there is a singularity at the origin, cf the denominator of equation (23). Although the point kernel value is infinite at the origin, integrals over finite volumes are always finite. The physical interpretation of the singularity is best understood in terms of particle track density of primary released electrons. Since they all stem from one point, the track density becomes infinite and so does the dose, given constant ionization per track length. Also, photon pencil kernels are singular along the symmetry axis since the track density becomes infinite with all primary electron tracks originating from the axis. Special methods for kernel rebinning based on an energy conservative

volume overlap technique have been proposed by Eklöf *et al* (1990). For Cartesian- cylindrical conversions, Rathee *et al* (1993) used interpolating functions renormalized within each original bin to improve the rebinned result.

Direct experimental validation of point kernels is not possible because one cannot force photon interactions to take place at a single location in an extended absorber. However, the reciprocity principle can be applied to design experiments as carried out by O'Connor and Malone (1989). Recently, pencil beam dose kernels were determined for 6 and 25 MV x-rays by fitting analytical models to quantities derived from broad beam data (Ceberg *et al* 1996). Iwasaki derived *forward and backward spread functions* from measured data in water to calculate primary and scatter dose separately (Iwasaki 1985, Iwasaki and Ishito 1984).

Energy deposition kernels are invaluable tools for understanding qualitative aspects of dose distributions. At low energies (< 1 MeV), the electron range is very much shorter than the photon mean free path. A considerable portion of the primary photon energy is also further transported to yield scatter dose as shown in figure 7. At very high energies such as 50 MeV the electron track lengths are of the same order as the photon mean free paths and only a minor part of the primary photon energy is transferred to scatter dose as illustrated in figure 7.

7.2. Point kernel models

The calculation of dose from point kernels can be described as a two-step procedure as sketched in figure 8. In the first step the energy released in the patient through attenuation of the primary photons is calculated by ray-tracing primary photon trajectories, including beam modulators, etc. The raytrace is normally performed in a Cartesian matrix (cf Siddon 1985) with interaction data mapped from CT scans to represent the patient. In the second step, dose is calculated by superposition of appropriately weighted kernels. Following the common kernel normalizations in equation (21), the dose equation for monoenergetic irradiation of a homogeneous phantom with a parallel beam follows as

$$D(\boldsymbol{r}) = \iiint_V T(\boldsymbol{s})h(\boldsymbol{r}-\boldsymbol{s})\,\mathrm{d}^3s \tag{24}$$

where $T(\boldsymbol{s})$ is the *terma* (*t*otal *e*nergy *r*eleased per *ma*ss (Ahnesjö *et al* 1987)) from the primary photon energy fluence $\Psi(\boldsymbol{s})$ in the volume element d^3s. The integration variable $\boldsymbol{s}$ in equation (24) is terma oriented and the purpose of the kernel is to weight the energy transfer from all irradiated $\boldsymbol{s}$ to $\boldsymbol{r}$.

Through variable substitution, equation (24) is equivalent to

$$D(\boldsymbol{r}) = \iiint_V T(\boldsymbol{r}-\boldsymbol{s})h(\boldsymbol{s})\,\mathrm{d}^3s \tag{25}$$

in which the integration variable $\boldsymbol{s}$ is kernel oriented and the kernel weights the energy transfer from all $\boldsymbol{r}-\boldsymbol{s}$ to $\boldsymbol{s}$. The reciprocity between photon interaction and dose deposition sites has been discussed by Hoban *et al* (1994), cf section 2.3. When equations (24) or (25) are computer coded as discrete summations to yield dose distributions as a function of $\boldsymbol{r}$, one has to loop over the locations of both $\boldsymbol{s}$ and $\boldsymbol{r}$. Choosing the loops over the $\boldsymbol{r}$ locations to be outermost yields dose values point by point. If instead the outermost loops are chosen to be over the $\boldsymbol{s}$ locations the dose distribution is gradually built up and no point dose values are ready until the full distribution is ready. Mackie *et al* (1985) labelled these different loop orders after

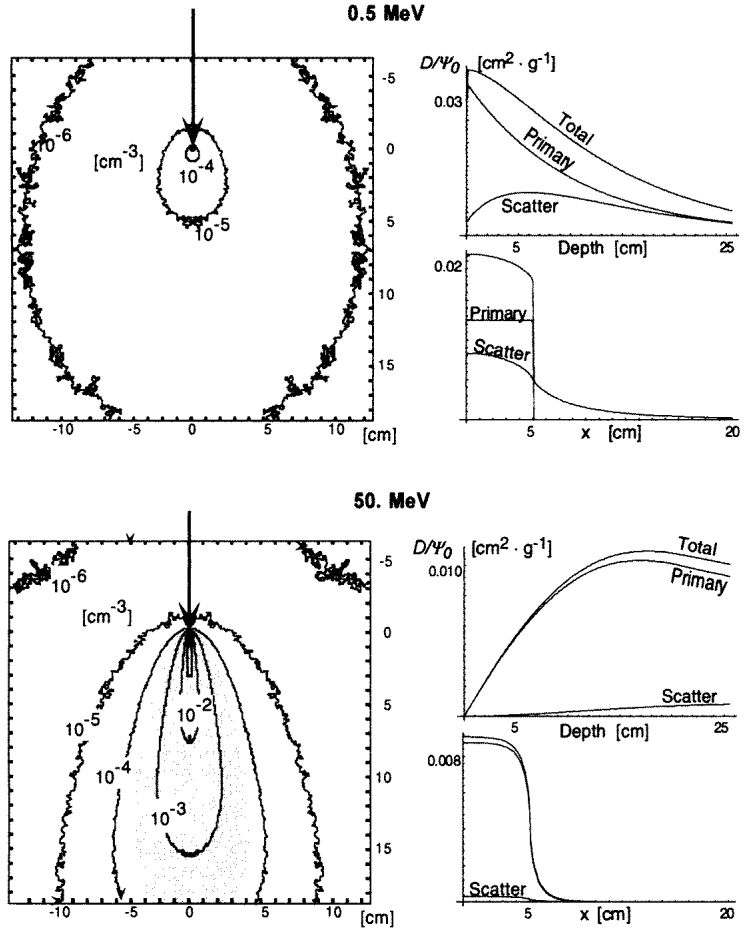

Figure 7. Point kernels in isolevel format (left) and depth doses and profiles (right) for a $10 \times 10\ cm^2$ field at infinite SSD. The grey area of the 50 MeV point kernel shows the lateral extension of the primary dose. The corresponding area at 0.5 MeV is so small that it is not resolved (from Ahnesjö 1992).

the outermost loops as the '*dose deposition point of view*' and the '*interaction point of view*' respectively.

The dose equation (24) is exactly valid for an arbitrary distribution of the fluence of monoenergetic photons incident in a parallel beam on an infinite medium—a highly idealized situation. We will in the following sections discuss the adaptation of point kernel methods to more general conditions.

7.2.1. Basic generalizations and approximations. As reviewed by Battista and Sharpe (1992), the considerations that impose approximations to point kernel superposition models are (a) the spectral and geometrical properties of clinical x-ray sources, (b) the heterogeneous medium of finite extent (a patient!) and (c) the time constraints imposed by interactive treatment planning.

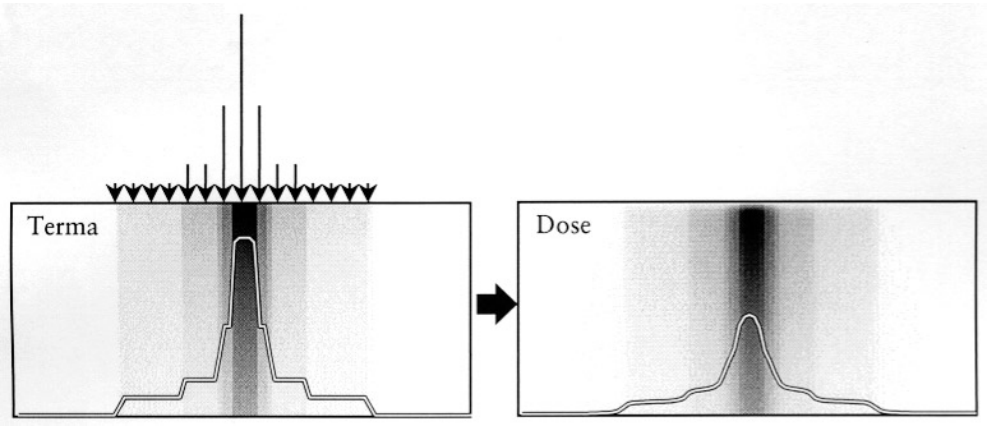

Figure 8. The initial step (left) of point kernel models is to ray trace the incident beam for calculation of the energy transferred to secondary particles, i.e. the terma. In a subsequent step the energy of the secondary particles are transported and deposited as dose (right). Due to the energy transport by secondary particles, dose patterns are always smoother than the corresponding patterns of primary beam energy release.

7.2.1.1. Generalization for primary beam spectral variations. Polyenergetic beam sources (cf section 9.1.1) can be considered by generalizing equation (24) to

$$D(\boldsymbol{r}) = \int_E \iiint_V T_E(\boldsymbol{s}) h(E, \boldsymbol{r} - \boldsymbol{s})\, \mathrm{d}^3 s\, \mathrm{d}E \tag{26}$$

where the energy dependency is included by using an energy-dependent kernel and terma differential in energy. Here, the terma differential in energy is given by

$$T_E(\boldsymbol{r}) = \frac{\mu}{\rho}(E, \boldsymbol{r}) \Psi_E(\boldsymbol{r}) \tag{27}$$

where $\mu/\rho(E, \boldsymbol{r})$ is the mass attenuation coefficient of the primary photons of energy E and $\Psi_E(\boldsymbol{r})$ the energy fluence, differential in energy, of primary photons at $\boldsymbol{r}$. Terma calculation and subsequent superposition over an energy dimension require repeated spatial integrations (see equation (26)) and is computationally expensive. Representing the energy spectrum with a single (mean) energy does not result in accurate depth dose values. Boyer *et al* (1989) found that five energy bins were enough to represent the spectrum for a 6 MV Siemens machine. Five bins were also used by Zhu and Van Dyk (1995) who investigated the sensitivity in depth dose from variations in each spectral bin. Hence, a straightforward discrete implementation of equation (26) requires that the spatial convolution must be repeated at least five times with considerable timing drawbacks. The spectrum variations to consider are (a) 'depth hardening' of the primary beam due to filtration in the irradiated object and (b) 'off-axis softening', i.e. lateral variation of the spectrum due to decreasing beam hardening in the flattening filter with off-axis distance, cf Lee (1997). Several approaches have been proposed to circumvent the need for explicit calculations for each energy interval.

For depth hardening, Metcalfe *et al* (1989, 1990) concluded that terma is the major factor in determining the shape of the calculated dose distribution. Therefore, in polyenergetic beams, it is important to include spectral influence on the terma distribution. Papanikolaou *et al* (1993) carried out a full calculation for polyenergetic terma and showed that a polyenergetic kernel should be averaged using terma-weighted contributions for the spectral bins. Beam hardening

effects on the polyenergetic kernel were accounted for by applying a precalculated depth-dependent correction factor derived from the ratio of depth dose curves obtained from a full calculation (equation (26)) and the single polyenergetic kernel superposition. Liu *et al* (1997c) replaced the correction factor by use of a kernel, interpolated for each depth from polyenergetic terma-weighted kernels pre-calculated for the surface and two more depths. However, attenuation coefficients, and consequently also terma distributions and kernels (in the normalization according to equations (21) and (22)), are only weakly dependent on energy (Ahnesjö 1987, Ahnesjö *et al* 1987). Hence, Hoban *et al* (1994) and Hoban (1995) proved that the separation of the energy diffusion process into a primary dose convolution and a scatter dose convolution, suggested by Ahnesjö (1991), yields very accurate results. In essence, they made the following approximation

$$\begin{aligned} D(\boldsymbol{r}) &= \int_E \iiint_V T_E(\boldsymbol{s}) h(E, \boldsymbol{r}-\boldsymbol{s})\,\mathrm{d}^3 s\,\mathrm{d}E \\ &\approx \iiint_V P(\boldsymbol{s})\tilde{h}_{\mathrm{p}}(\boldsymbol{r}-\boldsymbol{s})\,\mathrm{d}^3 s + \iiint_V S(\boldsymbol{s})\tilde{h}_{\mathrm{s}}(\boldsymbol{r}-\boldsymbol{s})\,\mathrm{d}^3 s \end{aligned} \tag{28}$$

where the released energy distributions for primary, P (i.e. the collision kerma), and scatter, S, are given by

$$P(\boldsymbol{r}) = \int T_E(\boldsymbol{r})\frac{\mu_{\mathrm{en}}}{\mu}(E)\,\mathrm{d}E \tag{29}$$

$$S(\boldsymbol{r}) = \int T_E(\boldsymbol{r})\left(1 - \frac{\mu_{\mathrm{en}}}{\mu}(E)\right)\mathrm{d}E \tag{30}$$

with the corresponding kernels (cf equation (22)) weighted by the terma at a certain depth z_0 and renormalized through

$$\tilde{h}_{\mathrm{p}}(\boldsymbol{r}) = \frac{\int \Psi_E(z_0)\mu(E)h_{\mathrm{p}}(E,\boldsymbol{r})\,\mathrm{d}E}{\int \Psi_E(z_0)\mu_{\mathrm{en}}(E)\,\mathrm{d}E} \tag{31}$$

$$\tilde{h}_{\mathrm{s}}(\boldsymbol{r}) = \frac{\int \Psi_E(z_0)\mu(E)h_{\mathrm{s}}(E,\boldsymbol{r})\,\mathrm{d}E}{\int \Psi_E(z_0)(\mu(E)-\mu_{\mathrm{en}}(E))\,\mathrm{d}E} \tag{32}$$

to yield unity integrals over infinite space. The separation enables the study of primary and scatter dose separately and also provides the means for straightforward implementation of off-axis softening corrections (Saxner and Ahnesjö 1998). The kernel definition depth z_0 used by Hoban *et al* was set to the phantom surface, but an arbitrary depth such as 10 cm can be used with insignificant difference in calculated dose. Hoban (1995) also showed that beam hardening translates to an (almost linear) increase of the mean primary photon energy with depth and the consequence of this is shown to be a linear increase of the ratio of collision kerma to terma with depth. Terma calculation time can be a significant part of the overall dose calculation time (Reckwerdt and Mackie 1992) and the linearity can be exploited to simplify calculations of the P and S distributions respectively.

7.2.1.2. Beam divergence. For divergent beams, there is an inverse square factor reduction of the primary photon fluence with depth, a linear increase of each field dimension with depth and a rotation, 'tilting', of the kernels (see figure 9). Papanikolaou *et al* (1993) investigated the approximation of applying the inverse square correction outside of the inner summation loop to increase computation speed, i.e. the inverse square correction is applied at the dose deposition site instead of the primary interaction site. It was found

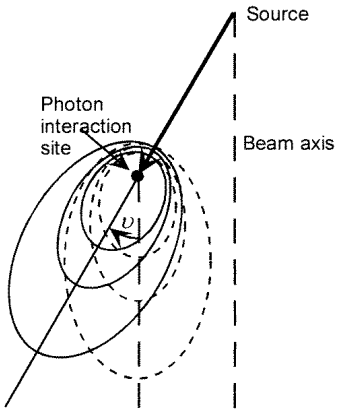

Figure 9. Kernels should ideally be 'tilted' by an angle ν versus the beam axis to align with the primary photon direction at the interaction site.

that approximation compensates for not aligning kernels to the fan-like geometry of the beam. Many implementations neglect the effect of kernel tilting and a study on the validity of parallel kernel approximation was carried out by Sharpe and Battista (1993). They found that in combinations of extreme cases such as small SSD, large field size and high energy, errors above 3% are likely to be observed. Locally in penumbras larger errors are generated as artefacts. Nevertheless, they concluded that using parallel kernels was an acceptable approximation for most clinical situations. Liu *et al* (1997c) made detailed comparisons of different approaches to kernel tilting and pointed out that the computation of the tilt angle ν is most efficiently calculated in the 'dose deposition point of view' since a complete coordinate transform between the kernel system and the beam system can be avoided.

7.2.1.3. Tissue heterogeneity density scaling and finite patient extent. The transfer of energy by first scatter photons depends on the constitution of the medium between the primary photon interaction site and the dose deposition point. The deposition of energy mediated by multiply scattered particles depends on the medium located elsewhere, but it depends more on the medium close to the initial direction then on media far off, since the scattering cross sections are largest in the forward direction. This justifies the common approach of scaling all dose fractions of a point kernel h_{ρ_0}, calculated for a homogeneous medium of mass density ρ_0, by the mean electron density between the point $\boldsymbol{s}$ of energy release and the point $\boldsymbol{r}$ of energy deposition, i.e.

$$h_{\text{het}}(\boldsymbol{s}, \boldsymbol{r}) = \frac{\rho(\boldsymbol{r})}{\rho_0} c^2 h_{\rho_0}[c(\boldsymbol{r} - \boldsymbol{s})] \tag{33}$$

where

$$c = c(\boldsymbol{s}, \boldsymbol{r}) = \int_0^1 \rho_{\text{rel}}[\boldsymbol{s} - \ell(\boldsymbol{s} - \boldsymbol{r})]\,\mathrm{d}\ell \tag{34}$$

in which ρ_{rel} is the relative number of electrons per volume as compared with the reference medium. The convolution integral in equation (24) is then replaced by the superposition

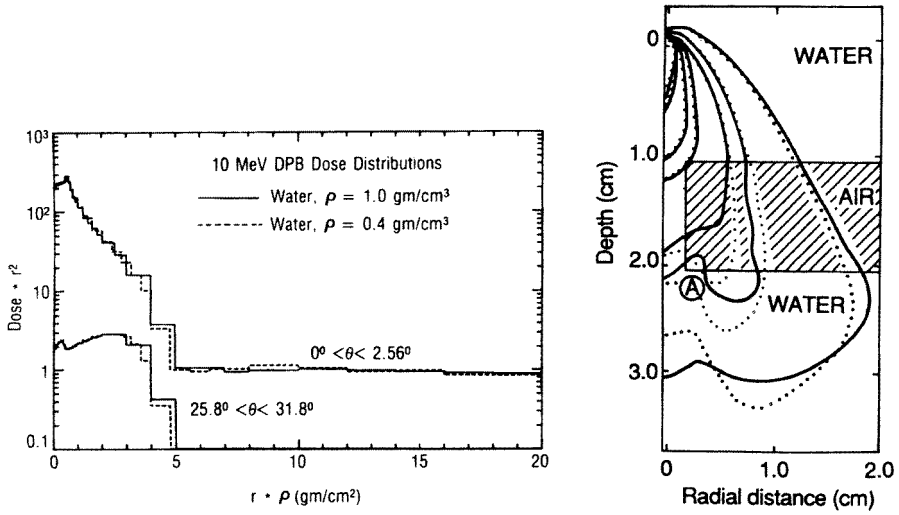

Figure 10. Left: Comparison of density scaled point kernels in homogeneous media with kernels generated directly with Monte Carlo. Data are presented along radial lines out from the interaction centre and multiplied by the radius squared. (From Mohan *et al* (1986), with permission.) Right: Comparison in isolevel format of a density scaled point kernel (dotted) and a Monte Carlo kernel (full) in a heterogeneous geometry with an air ring. The largest deviation was found to be at point A. (From Woo and Cunningham (1990), with permission.)

integral

$$D(\boldsymbol{r}) = \iiint_V T(\boldsymbol{s}) \frac{\rho(\boldsymbol{s})}{\rho_0} c^2 h_{\rho_0}[c(\boldsymbol{r} - \boldsymbol{s})] \, \mathrm{d}^3 s. \tag{35}$$

This scaling has been evaluated by Mohan *et al* (1986) (see figure 10) and is consistent with the theorems of O'Connor and Fano. The density scaling is used to avoid the tedious task of calculating an 'exact' kernel for every situation. The problem has also been investigated by Woo and Cunningham (1990) who compared Monte Carlo kernels for a sample of inhomogeneous geometries with density scaled *water* kernels. They concluded that although the deviations between the kernels could locally be substantial, as shown in figure 10, the overall effect on dose was less severe due to averaging from surrounding kernels. Density scaling of a discrete kernel is numerically the same type of problem as the rebinning of a homogeneous kernel into bins of sizes as scaled according to the inhomogeneities. This requires special care in high-gradient regions, cf discussion on rebinning in section 7.1. The effect of high kernel gradients is probably the main reason for differences in results from apparently equivalent methods of kernels as reported by Wong and Purdy (1990).

For the primary dose kernels, two groups have worked towards improving the density scaling procedures by employing the Fermi–Eyges electron scattering theory. Keall and Hoban (1995) extended the rectilinear density scaling method by multiplying c in equation (36) with a factor based on the Fermi–Eyges calculated lateral planar fluence distribution. Although this extra scaling was implemented in the direction of the beam axis only, the results improved as shown in figure 11, but with an increase in calculation time by a factor of 3. Yu *et al* (1995) proposed to transport the electrons separately, by an electron pencil beam model in which the medium is approximated as layered along the transport direction. This was also shown to model well the effect on dose due to the presence of materials with different atomic

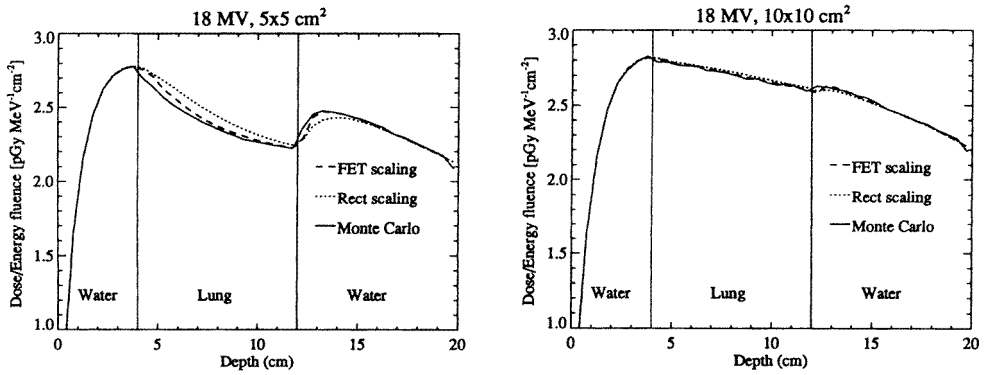

Figure 11. Depth dose curves for a 5×5 cm^2 beam (left) and a 10×10 cm^2 beam (right), for 18 MV in a water–lung–water phantom. Results of Monte Carlo (full curves), rectilinear density scaling of point kernels (dotted curves), and electron fluence scaling based on Fermi–Eyges theory (dashed curves) are shown. (From Keall and Hoban (1995), with permission.) The error from density scaling of the primary dose vanishes when the electrons contributing dose to a point originate within the same density regions.

numbers. Sauer (1994, 1995) suggested a method that considered the difference in stopping power and range between water and a high atomic number (Z) material, where the energy deposited in the high-Z material is calculated by rectilinear path scaling using the mean mass stopping power ratio of the high-Z material to water and by multiplying the energy deposition value with the mass stopping power ratio at the site. In addition, to account for the increased lateral diffusion of electrons in the high-Z material, the energy deposited was adjusted by averaging with energy deposited at adjacent angular positions. Recently, Keall and Hoban (1996a) proposed a method where they circumvented the kernel scaling problem by explicitly transporting electrons using pre-generated Monte Carlo electron track data. This required prolonged calculation times, a factor of 30 as compared with a straightforward kernel superposition.

The dose deposited through multiply scattered photons was considered by Boyer and Mok (1985) to be rather diffused and they employed a diffusion theory for modelling dose from these photons. Similarly, Mackie *et al* (1985) chose, according to the average density, an appropriate scatter kernel from a database of kernels generated in water-like media of different densities. Kernel representation of the dose from multiply scattered photons is also affected by the common approximation of using a very large, or infinite, phantom while generating the kernel. This will result in an overestimation of the dose near media boundaries, such as in cases of tangential irradiation, due to photons considered to be backscattered through the surfaces facing empty space as if it was water everywhere. Superposition calculations for a 4 MV beam in a 'half phantom' geometry (without surface curvature) have demonstrated errors of several per cent within the first 3 cm from the phantom edges (Aspradakis 1996). At higher energies, however, the kernel distributions are more forward directed and dose due to multiply scattered photons is less and the error decreases. A detailed investigation on photon beam exit dose was carried out for ^{60}Co and 24 MV beams by Woo (1994). He confirmed the findings of Mohan *et al* (1986), namely that a convolution calculation using an invariant kernel underestimates the dose drop at the beam exit surface due to a reduction of backscatter not being accounted for.

7.2.2. Calculation algorithms. Despite the continuous rapid development of computers with ever- increasing computational speed, straightforward application of kernel superposition is still time consuming enough to impede its full implementation into clinical routine. Several projects have demonstrated speed improvement by use of specialized hardware (cf Murray *et al* 1991, McGary and Boyer 1997). Although photon transport has an inherent parallelism, the increasing system complexity and lack of standardization has so far limited the use of specialized parallel architectures in commercial treatment planning systems. Hence, there has been an intense search for effective algorithms to speed up calculations, especially since the demand for dose computations in treatment planning is foreseen to increase from a more widespread use of iterative optimization methods.

7.2.2.1. Direct summation. Several methods can be used for direct summation of density scaled kernels in dose calculations. Straightforward discrete implementation of equation (24) in a homogeneous medium requires N^6 multiplications and summations to calculate the result to N^3points. The inclusion of kernel scaling as in equation (35) will further increase the number of operations to N^7. Direct summation is therefore very time consuming, and several techniques and approximations have been explored in order to increase the calculation speed. These include the use of Fourier transforms, the collapsed cone approximation and correction factor interpolation.

7.2.2.2. Fast transform techniques. The use of fast transform convolution techniques, such as the fast Fourier transform (FFT), to carry out the discrete convolution (Ahnesjö 1984, Boyer and Mok 1984, 1985, Murray *et al* 1989) scales the number of operations for the homogeneous case essentially with the 3D Fourier transform requiring $3N^2$ 1D transforms each of $N \log_2 N$ operations, i.e. the approach scales as $N^3 \log_2 N$ instead of the direct summation proportionality N^6. Transform based fast convolutions require a spatially invariant kernel and several attempts have been made to circumvent the invariance requirement. Boyer and Mok (1986) proposed a method that scaled the scatter dose kernel by the density at the scatter site only. This method has been tested (Wong and Purdy 1990, Zhu and Boyer 1990) and found to yield encouraging results in a number of situations. The method has been improved (Ahnesjö 1987, Wong *et al* 1996) to include the densities at both the scattering and the receiving sites for scaling of the scatter kernel. However, all these methods fail to scale the primary dose due to high kernel gradients. The problem of lateral electron transport in FFT convolution has been studied further by Wong *et al* (1997) who presented an improvement on the calculation of primary dose along the central axis in cases of electronic disequilibrium and in the penumbra region by scaling field sizes at each depth with local effective densities. These are computed, in a manner resembling that used in the ETAR model, by convolving the density at the interaction site with the primary kernel for water.

7.2.2.3. Collapsed cone convolution. The collapsed cone method proposed by Ahnesjö (1989) applies an angular discretization of the kernel which, together with the parametrization in equation (23), enables an efficient approach for energy transport and deposition. Angular discretization of a parametrized point kernel yields, for each discrete angular sector (cone) Ω_i, the energy deposition per radial distance as

$$\iint_{\Omega_i} \frac{h_{\rho_0}}{\rho}(r, \Omega) r^2 \, \mathrm{d}^2\Omega = A_{\Omega_i} \mathrm{e}^{-a_{\Omega_i} r} + B_{\Omega_i} \mathrm{e}^{-b_{\Omega_i} r}. \tag{36}$$

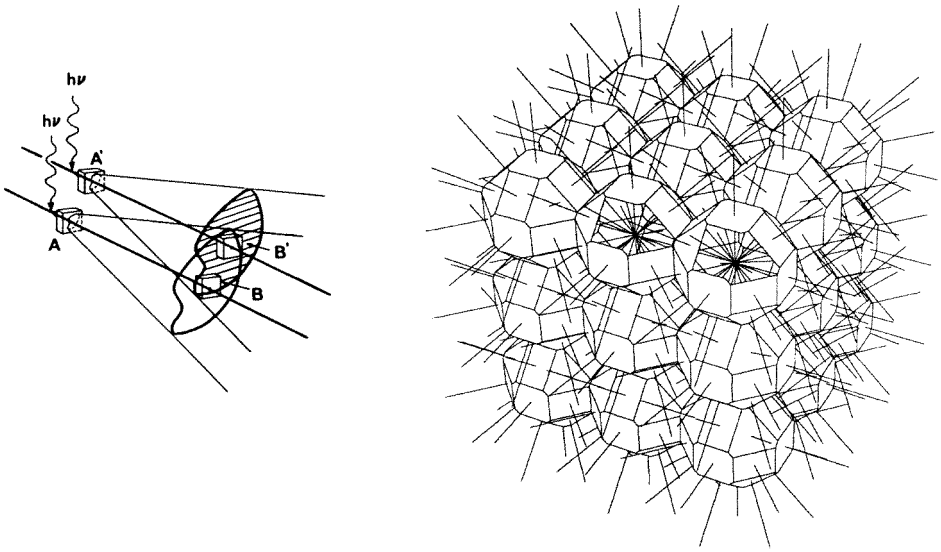

Figure 12. Left: A consequence of the collapsed cone approximation to transport the energy along a discrete axis is that the energy that should have been deposited in voxel B′, from interactions at the vertex of the lower cone, is deposited in voxel B and vice versa. This displacement grows with distance; however, the first scatter fraction decreases with increasing distance, making the approach acceptable as the total energy deposited is conserved. Most energy is deposited close to where it is released, making displacement errors less important since it takes place mainly within voxels, as shown by the voxels A and A′. (From Ahnesjö 1989.) Right: Example of a simple lattice of cone axes made to cover the $3 \times 3 \times 3$ calculation voxels with the 26 discrete cone directions used in this case. (From Ahnesjö 1991.) In this example all transport lines intersect at each voxel centre but this is not required (Reckwerdt and Mackie 1992) as long as each voxel is intersected by each direction.

Notice that the inverse square of the radius cancels due to the increasing cross section of the cone Ω_i with increasing radius. When the angular discretized kernel is convolved with the terma distribution, all energy released into the cone direction Ω_i from volume elements on the cone axis is approximated to be rectilinearly transported, attenuated and deposited in volume elements on that axis, i.e. the cones are *collapsed* onto their axes (see figure 12). A lattice of transport lines, representing cone axes, is constructed to cover the irradiated volume such that each direction intersects every calculation voxel. This requires a parallel subset of lines for each discrete direction of the 'collapsed' kernel, which can be arranged in several ways (Ahnesjö 1989, 1991, 1997, Reckwerdt and Mackie 1992) (see figure 12 for a simple example). Due to the exponential description of the kernel, the energy transport along a line can be expressed analytically resulting in recursive formulae that only need to be evaluated once for each voxel on that line. Kernel scaling for the heterogeneities is performed during the recursion, both for the primary and scatter dose kernels (i.e. both terms in equations (23) and (36)). The recursions pass each voxel at least once per direction. When each point is calculated individually, the number of operations will be proportional to MN^4, where M is the number of conical sectors (angular bins). If instead the dose is calculated in one sequence for a bulk of N^3 points the total number of operations needed in heterogeneous media is proportional to MN^3. In a similar method Reckwerdt and Mackie (1992) bypassed the exponential parametrization by using the result of an initial ray-trace along each transport line to look-up the radiological distance between each pair of release/deposition points. This

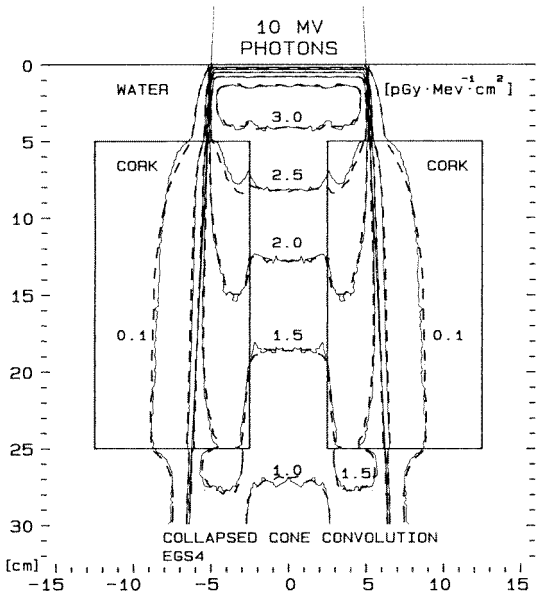

Figure 13. Dose from a 10×10 cm^2 10 MV beam in a lung phantom where the hatched isodoses show the result from collapsed cone calculations and solid isodoses the result from Monte Carlo. Note the penumbra broadening in lung and buildup after lung which is well reproduced using the collapsed cone approximation. (From Ahnesjö 1989.)

results in an MN^4 algorithm since for each point the other points on the same line have to be visited separately.

The collapsed cone convolution method has been verified against Monte Carlo generated dose distributions for slab and mediastinum-like phantom geometries (Ahnesjö 1989; see figure 13), and for clinical beams in homogeneous media (Lydon 1998), in both cases demonstrating generally very good results.

7.2.2.4. Correction factor interpolation. Aspradakis and Redpath (1997) devised a technique for reducing computation time in a superposition model. The method is based on the assumption that the conventional inhomogeneity correction method adequately predicts the shape of the dose distribution over a limited distance. Hence correction factors, defined as the ratio of dose values from superposition to those from the conventional (broad beam, fast, inhomogeneity correction) algorithm calculated on a coarse matrix and further interpolated onto a fine grid are applied to relative dose values calculated on the fine grid by the fast conventional method. This method requires the generation of two 3D matrices; one from the conventional model on a fine matrix and the other from superposition on a coarse matrix. The speed enhancement as compared with a full calculation approach depends on the resolution ratio. As an example, Aspradakis and Redpath demonstrated a 128-fold improvement in speed without significant loss in accuracy when the correction factor was carried out every 4.0 cm along the direction of the beam and every 2.0 cm across the beam in comparison to a grid separations of 0.5 cm in all dimensions. However, in regions of high dose gradients, a finer resolution might be required.

7.3. Pencil kernel models

A pencil kernel describes the energy deposited in a semi-infinite medium from a point monodirectional beam (see figure 6). For the purpose of treatment optimization, Gustafsson *et al* (1994) used a very general formulation of the radiotherapy dose calculation problem:

$$D(\boldsymbol{r}) = \iint_{s} \int_{E} \iint_{\Omega} \sum_{m} \Psi^{m}_{E,\Omega}(\boldsymbol{s}) \frac{p^m}{\rho}(E, \Omega, \boldsymbol{s}, \boldsymbol{r})\, \mathrm{d}^2\Omega\, \mathrm{d}E\, \mathrm{d}^2 s \tag{37}$$

where $\Psi^{m}_{E,\Omega}(\boldsymbol{s})$ is the energy fluence differential in energy E and direction Ω for beam modality m and $(p^m/\rho)(E, \Omega, \boldsymbol{s}, \boldsymbol{r})$ is the corresponding pencil kernel for energy deposition per unit mass at $\boldsymbol{r}$ due to primary particles entering the patient at $\boldsymbol{s}$. For routine dose calculations the approach of equation (37) is still impractical since the pencil kernel is variant and in principle unique for each combination of $\boldsymbol{s}$ and $\boldsymbol{r}$. In equation (37) the beam that yields this kernel is of infinitesimal cross section whereas in practice Gustafsson *et al* discretized the kernels to describe the energy deposition from divergent, finite width beam elements (often referred to as bixels) which converted the integral to a matrix multiplication form. The discrete pencil kernel problem has been studied in more detail by Bourland and Chaney (1992) and Ostapiak *et al* (1997). Their study was motivated by the potential savings in computation time for superposition models since use of pencil kernel models can be viewed as a 'pre-convolution' of point kernels over the depth dimension. The pencil kernels are commonly determined using Monte Carlo methods, either directly or as a superposition of point kernels. Monte Carlo methods have been used by a number of workers (Mohan and Chui 1987, Ahnesjö and Trepp 1991, Ahnesjö *et al* 1992b, Bourland and Chaney 1992). Pencil kernels have also been estimated experimentally using scatter factor differentiation (Ceberg *et al* 1996, Storchi and Woudstra 1996).

The integration over the field aperture is greatly simplified by use of spatially invariant kernels and various techniques have been developed to numerically evaluate such integrals. When the lateral dose distribution at a particular depth is of interest, standard convolution methods using transforms can be applied (Mohan and Chui 1987, Ahnesjö and Trepp 1991). Bortfeld *et al* (1993) showed that the dose at arbitrary points can be interpolated from two profiles, essentially representing primary and scatter dose, using a depth dependent weighting technique derived from a singular value decomposition of the kernel data. Storchi and Woudstra (1996) combined a pencil kernel approach by computing a sparse lattice of points using transform technique with an interpolation along beam lines to reconstruct dose at arbitrary points. Ahnesjö *et al* (1992b) noted that pencil kernels, expressed in cylindrical coordinates (r, z), can be accurately parametrized as

$$\frac{p}{\rho}(r, z) = \frac{A_z \mathrm{e}^{-a_z r} + B_z \mathrm{e}^{-b_z r}}{r} \tag{38}$$

where A_z, a_z, B_z and b_z are functions of depth. They also developed a numerical integration technique based on a combination of the parametrization with a triangular decomposition of the field shape (similar to that of Siddon *et al* (1985)), and fluence weighting to allow for both intensity modulation and complicated field shapes.

Pencil kernel models are effectively hybrid algorithms that fully account for beam modulations and field shapes but rely on broad beam scaling/correction methods to handle heterogeneities and patient outlines (cf section 5.1.1). Provided there are properly normalized fluence and kernels, the dose is calculated in absolute units that can be used to derive output factors. The two main accuracy limitations on pencil kernel models are for heterogeneities (Knöös *et al* 1995) and for scatter dose calculations in phantom sizes that deviate substantially from the size for which the pencil kernel is determined (Hurkmans *et al* 1995). Nevertheless, the

inherent flexibility to model lateral fluence variations combined with computational efficiency has made the pencil kernel method popular, in particular for use in optimization of intensity modulation (Bortfeld *et al* 1994, Gustafsson *et al* 1994, Söderström *et al* 1993, Chui *et al* 1994).

8. Explicit modelling of scattered particle transport

8.1. Random methods, Monte Carlo

The widespread use of Monte Carlo applications in medical physics has been reviewed by Mackie (1990) and Andreo (1991). Photons have a limited number of interactions before they are absorbed, which makes it easy to simulate all interactions directly. In electron transport, however, the number of Coulomb interactions with atomic nuclei is so large that a direct Monte Carlo simulation is impractical. This has motivated the development of 'condensed' history techniques where different 'microscopic' interactions are classified into groups to provide a detailed 'macroscopic' representation of the particle transport (Berger 1963). The condensing assumes the medium to be locally homogeneous, making it non-trivial to study interface effects in detail. The grouping may be implemented in different ways using different approximations (Andreo and Brahme 1984, Bielajew and Rogers 1987, Kawrakow and Bielajew 1998). Dose scoring for treatment planning is, however, not as critical as simulation of ionization chamber responses. Hence, Monte Carlo is considered to be the primary method for bench-marking of faster dose calculation approaches.

For photon beam dose calculation, the long mean free paths between interactions means that the energy is transferred to the medium in local fractions over large volumes and necessitates simulation of a very large number of photon histories to reduce statistical uncertainty. The secondary electrons released by the photons smooth the dose distribution, which is more efficient at higher energies due to longer electron tracks. Hence, Monte Carlo is more efficient at higher photon energies than at lower energies making brachytherapy sources the most demanding candidate for direct use of Monte Carlo dose calculations. Long calculation times are a pronounced problem in conformal therapy where optimization of dose distributions using iterative algorithms requires the dose to be recomputed many times during the planning procedure. Hence, it is likely that for another decade photon Monte Carlo will be used for beam characterization, benchmarking and other special studies rather than routine treatment planning. Nevertheless, a very ambitious Monte Carlo treatment planning project has been launched at the Lawrence Livermore Laboratory aiming to model all beam modalities, including photons, by means of stand-alone machines networked to the treatment planning computer (Hartmann Siantar *et al* 1997). Based on the EGS4 code, Wang *et al* (1998) proposed to improve efficiency through the use of variance reduction techniques and density thresholding, the latter to speed up the ray-tracing calculations. For electron beams, several projects report clinical or near-clinical implementations for direct use in treatment planning (Manfredotti *et al* 1990, Neuenschwander *et al* 1995, Keall and Hoban 1996b, Kawrakow *et al* 1996), and it is likely that Monte Carlo calculations will be the clinical workhorse for electron beam calculations in the near future.

8.2. Deterministic methods for particle transport

The most general description of a radiation field at a given time is the phase space density, i.e. the number of particles per six-dimensional 'volume' made up of the three spatial coordinates $\boldsymbol{r} = (x, y, z)$, the particle energy E and the direction $\Omega = (\theta, \phi)$. Since the particles of a

radiation beam actually move, the phase space can be completely represented by the vectorial energy fluence differential in energy and direction for photons, $\Psi^{\mathrm{ph}}_{E,\Omega}$, and for charged particles (electrons and positrons), $\Psi^{\mathrm{cp}}_{E,\Omega}$. A number of quantities of dosimetric interest can be derived directly from these fluences and in particular the dose follows according to Rossi and Roesch (1962)

$$D(\boldsymbol{r}) = -\frac{1}{\rho(\boldsymbol{r})}(\nabla \cdot \Psi^{\mathrm{ph}}_{E,\Omega}(\boldsymbol{r}) + \nabla \cdot \Psi^{\mathrm{cp}}_{E,\Omega}(\boldsymbol{r}) - q(\boldsymbol{r})) \tag{39}$$

where ρ is the mass density and q the rest mass changes. From a given initial radiation field, continuity laws, as expressed in the well known Boltzmann equation, govern the resulting fluence distributions. The scattering and absorption processes make the Boltzmann equation difficult to solve except for very simplified cases. Bellman and co-workers (see Bellman and Wing (1975) for an introduction) have made theoretical studies proposing the use of an invariant embedding technique to solve the radiation transport problem in slab geometries. A more general method to numerically solve the Boltzmann equation is the method of discrete ordinates which discretizes the spatial dimensions into voxels, the directions into 'discrete ordinates' (as for the collapsed cone method; cf section 7.2.2.3) and the energy range into 'multigroups' (see Bell and Glasstone (1970) for a general introduction). The discrete ordinates, or S_N, method has long been used for neutron transport calculations in nuclear engineering, and code packages such as DANTSYS are generally available (Alcouffe *et al* 1995). The method has not attracted much interest in the medical physics community and there are only a limited number of papers available including those by Shapiro *et al* (1976) who investigated ^{252}Cf as a brachytherapy source, Uwamino *et al* (1986) who calculated neutron leakage from a medical electron accelerator, Nigg *et al* (1991)who investigated dose distribution analysis in boron neutron capture therapy and Gokhale *et al* (1994) who focussed on inverse methods for beam direction selection in 2D planning. The method is only suited to problems where the particles are subject to a limited number of interactions before coming to rest since the number of iterations is proportional to the number of interactions. Hence, to completely solve the dose deposition in photon beams numerically by purely deterministic methods the electron transport must be solved by a more suitable method such as the phase space evolution originally developed for dose calculation in electron beams (Huizenga and Storchi 1989, McLellan *et al* 1992, Janssen *et al* 1997). The complexity and computational burden for such a complete deterministic approach would probably exceed that of the Monte Carlo approach (Börgers 1998).

9. Beam phase space characterization

Empirical dose calculation models use measured dose data almost directly in calculations. Hence, self-consistency with respect to measured beam data is intrinsic to empirical methods. For more explicit modelling of the radiation energy transport one needs a description of the initial phase space delivered by the beam, i.e. the time-independent energy fluence $\Psi_{E,\Omega}$ differential in energy and direction at all points (x, y, z_0) in a beam reference plane at z_0. However, there are no established methods to determine experimentally such a complete description in the clinical environment. Hence one must use either direct calculations based on the design of the machine or indirect methods based on simple measurable quantities such as dose distributions in a water phantom. In practice it is common to use a combination of both approaches. An excellent review of beam characteristics for both photon and electron beams has been published by Ebert *et al* (1996). The review given here will focus on work applicable to treatment planning with first-principle models.

Monte Carlo simulation of beam transport through clinical treatment heads has proved to be an invaluable tool to determine otherwise inaccessible data. The Monte Carlo approach has recently been greatly facilitated by Rogers *et al* (1995) who introduced the BEAM package tailored to simulate treatment heads by means of the EGS4 code (Nelson *et al* 1985). A similar package has also been designed by Lovelock *et al* (1995). The BEAM package has been used in a series of papers by Liu *et al* (1997a, b, d, 1998) to provide detailed information about phase space distributions for clinical machines. The Monte Carlo system GEANT, developed at CERN, has interfaces to mechanical engineering CAD (computer aided design) systems for handling complex designs. The GEANT system has been utilized by Küster *et al* (1997, 1998) to study multileaf collimators. A shortcoming of Monte Carlo for beam characterization is that the energy of the electron beam hitting the target is often not directly known with the required accuracy. Boyer *et al* (1989) determined the electron beam energy through a calibration of the bending magnet current and found deviations as high as 20% from the specified energy. A practical problem regarding Monte Carlo is that the set up of the simulations requires detailed geometrical knowledge of treatment head details which is not always easily accessible from manufacturers.

First-principle models give the absolute dose per impinging energy fluence. In practice the fluence monitoring is non-trivial since scattered photons from the treatment head add an 'unmonitored' contribution to the fluence, and backscatter into the monitor yields a 'false' contribution to the total signal (cf section 4.1):

$$\frac{\Psi}{M} = \frac{\Psi_0 + \Psi_{\mathrm{hsc}}}{M_0 + M_b}. \tag{40}$$

It is therefore common to describe the unscattered beam and the scattered components of the beam separately, as we will do in the following sections.

9.1. Primary fluence characterization

9.1.1. Beam spectrum and attenuation. Direct Monte Carlo simulations of the treatment head design have been carried out by several workers in order to provide spectral data. Mohan *et al* (1985) calculated, for a series of beam energies, spectra that later were frequently used as a standard set. They also studied the lateral variation in beam spectrum and characterized it in terms of half-value thickness. Lovelock *et al* (1995), Liu *et al* (1997d) and DeMarco *et al* (1998) (who used the MCNP code, (Briesmeister 1988)) applied Monte Carlo techniques to generate beam spectra and they all found that the incident electron beam energy must be tuned in order to get agreement with measured depth dose data.

Deterministic semianalytical calculations model the bremsstrahlung process as an electron diffusion and absorption with simultaneous emission of photons. The most energetic photons are generated in the direction of the electrons. Although the intensity is strongly forward peaked in the initial direction of the electrons, the angular dispersion of the electrons due to multiple scattering makes the unfiltered beam spectrum fairly uniform over the beam aperture. The subsequent filtering to flatten the fluence induces a slight variation such that the peripheral parts are softer due to thinner filters. Examples of works that apply this kind of model are Nordell and Brahme (1984), Ahnesjö and Andreo (1989), Desobry and Boyer (1994), Silver (1994) and Svensson and Brahme (1996). Deterministic models of the bremsstrahlung emission often apply Shiff's formulae as given in the classical review by Koch and Motz (1959). Desobry and Boyer (1991) reviewed the Shiff work and were able to relax some of the approximations that Shiff used.

Reconstructive techniques based on measured depth dose distributions are an appealing approach since the dose calculated using such spectra describes measured data as closely

as possible. To implement such a procedure a database of depth dose distributions from monoenergetic photons calculated by Monte Carlo must be available. The main difficulty in reconstructive techniques from depth dose distributions or attenuation measurements is the poor numerical conditioning of photon spectrum unfolding, which makes the use of different constraints necessary. Furthermore, the dose from charged particle contamination in the buildup region complicates the use of data from that region including the depth of dose maximum. Ahnesjö and Andreo (1989) combined a parametrized model for charged particle contamination with a semianalytical spectrum model whose parameters were varied to minimize the difference between measured depth doses and depth doses reconstructed as the sum of the dose for a pure photon beam and the charged particle dose. In a similar dose reconstructive approach Sauer and Neumann (1990) used general shape properties of realistic spectra expressed as positivity and monotony requirements. Attenuation data are more generally accessible than monoenergetic depth dose distributions and several reconstructive techniques based on attenuation measurements have been proposed (Huang *et al* 1983, Archer *et al* 1985, Piermattei *et al* 1990, Baker *et al* 1995, Baker and Peck 1997, Francois *et al* 1997, Nisbet *et al* 1998). Most of these works also used constraints on the spectral shape to handle numerical conditioning problems.

Methods for direct measurement of photon spectra, although not directly applicable in clinical environments, are of importance for benchmarking other methods. In particular, the data measured by Faddegon *et al* (1990, 1991), who also compared their data with Monte Carlo calculations, have become a standard.

In kernel based dose calculations the spectrum is often assumed to be laterally invariant. This approximation implies that off-axis softening, i.e. the decrease in energy with increasing angle versus the beam axis caused by decreasing flattening filter thickness, is ignored. For point kernel calculations this can be relaxed by considering the effects on the released energy fraction (collision kerma and scatter energy, i.e. equations (29) and (30)) through corrections describing the lateral change in beam penetration. Mohan *et al* (1985) used the angular distributions of photons generated by Monte Carlo techniques to compute off-axis changes in the half-value layer of water. In a broad experimental survey involving 15 different linac beams, Tailor *et al* (1998) showed that the relative change in the narrow beam half-value layer of water of the collated data was well described by a third degree polynomial of the off-axis angle. The earlier data from Yu *et al* (1997) and Bjärngard and Shackford (1994) were close to the data of Tailor *et al*. Although general parametrizations now exist, off-axis beam quality variations depend on the material of the flattening filter (Zefkili *et al* 1994) and should therefore be at least checked as part of the machine commissioning procedure.

9.1.2. Lateral fluence distribution. To achieve high accuracy, dose calculations must model the lateral fluence distribution as delivered by the open beam (not only for open beams but also as input for subsequent modulations of the beam). The common machine design paradigm is to shape the flattening system to deliver a uniform dose at some depth. Phantom scatter dose has its maximum at the beam centre, and the flattening system is designed to compensate for that by increasing the primary fluence with increasing radius (fluence 'horns'). In their Monte Carlo study, Lovelock *et al* (1995) pointed out that beam profiles were more sensitive indicators to variations of the electron beam energy than the depth dose curves. Hence, lateral profiles cannot entirely be predicted by Monte Carlo means and must be determined through measurements. Since detecting fluence is less developed than detecting dose, it is more common to use dose profiles and adapt the fluence profiles in calculations to fit measured dose rather than using measured fluence profiles. Boyer *et al* (1989) and Liu *et al* (1997d) assumed rotational symmetry characterized by a small set of profile measurements. Treuer *et al* (1987)

and Ahnesjö and Trepp (1991) worked out procedures to allow for full lateral mappings of general, non-rotational symmetrical beams. Ahnesjö and Trepp used radial dose scans rotated in 10° to 15° increments to achieve full mapping of the field. Most points are thereby taken in the 'curative region' and drifts in the experimental set-up are cancelled by renormalization to the beam axis point common to all scans.

9.1.3. Beam modulation. There are several methods for modulating the fluence of treatment units, as reviewed by Brahme (1987). The present most common technique is to use wedge shaped absorbers that influence not only modulation but also the beam quality. Hence, wedge factors expressed as fluence ratios will differ from wedge factors expressed as dose ratios. An important consideration in wedge dosimetry is the eventual effects the quality shifts have on different experimental techniques. Weber *et al* (1997) proved that buildup caps for detectors in fluence measurements could be made by any material when used *within* that same beam quality. Heukelom *et al* (1997) noted a difference in results between various cap materials when used for wedge factor determination. For dose calculations, Liu *et al* (1997b) ray-traced several energy bins through both the wedge and the patient. To reduce the number of ray-traces in the patient, Ahnesjö *et al* (1995) treated the quality shifts separately by correcting the separation of the released energies for the primary dose and scatter dose fractions, respectively, suiting the formalism as outlined by equations (28)–(32).

Modulation by dynamic collimation using the blocks, i.e. the dynamic wedge technique (Kijewski *et al* 1978), is relatively straightforward to model since the beam quality is not affected and excellent results have also been demonstrated (Weber *et al* 1996, Liu *et al* 1998, Storchi *et al* 1998). Somewhat more complicated to model is the modulation from multileaf blocks run in either 'step-and-shoot' mode (Bortfeld *et al* 1994, Webb 1998a, b) or in continuous mode (Convery and Rosenbloom 1992, Svensson *et al* 1994) since leaf interference yields spots with aberrant 'tongue-and-groove' underdosage and 'interleaf leakage' overdosage (van Santvoort and Heijmen 1996). At present there is great interest in exploiting the potentials in dynamic collimation motivated by the opportunities seen in treatment optimization utilizing non-uniform beams without increasing the labour cost of delivering the desired modulations.

9.2. Scatter from the treatment head

As stated in section 2, a significant amount of the treatment beam consists of scattered photons and secondary particles from practically all irradiated components of the treatment head. There is a large literature on experimental determination and empirical data fitting of quantities for 'output' characterization, intended for direct practical application. The magnitude and the relative importance of scatter from the various parts of the treatment head, however, have often been matter of confusion. The output factor in air is often called collimator scatter factor, indicating that the collimators are the most scattering parts. This is not the case, and it is now well established that the largest contributions originate in the flattening filter and close to the target in the primary collimator as experimentally showed through the work of Kase and Svensson (1986) and Jaffray *et al* (1993). For open beams on conventional machines, head scattered photons are of the order of one-tenth of the total energy fluence exiting the machine (Zhu and Bjärngard 1995, Weber *et al* 1997), with some additional per cent for wedged beams (Heukelom *et al* 1994, Liu *et al* 1997d). As noted by Weber *et al* (1997), some published output factors in air for high-energy beams do not describe the photon fluence output due to improper filtering of charged particle contamination. A common classification of head scatter sources, as given in the pioneering work of Nilsson and Brahme (1981) and Luxton and Astrahan (1988), is into scatter from the primary collimator (often merged into the flattening

filter component), the flattening filter, collimator backscatter into the monitor and collimator scatter. Nilsson and Brahme used Monte Carlo calculations and found the head scatter sources to be rather limited (<3%) while Luxton and Astrahan determined these experimentally and found them to be very important (<15%). These seemingly conflicting results are explained by the different treatment head configurations used in each work. Nilsson and Brahme used a configuration designed for a maximum beam diameter of 20 cm with a significantly thinner and hence less scattering flattening filter than that of typical clinical machines. Luxton and Astrahan used a CGR Saturne 25 machine which has a conventional flattening filter design but with collimator trimmers very close to the monitor chamber causing an unusually high amount of monitor backscatter. In the following, the treatment head scatter and related calculation models will be reviewed according to their source of origin.

9.2.1. Photon scatter from the flattening filter. The flattening filter forms an extended source distribution, which determines most of the variation of beam output in air due to variation of the field size. The filter is thickest at its centre. This, and the fact that the primary energy fluence at the exit side is approximately homogeneous, makes it natural to assume that the energy fluence of scattered photons is highest at the centre of the flattening filter and decreases towards the periphery. This has been shown experimentally (Jaffray *et al* 1993), analytically (Ahnesjö 1994) and with Monte Carlo simulations (Chaney *et al* 1994, Liu *et al* 1997d). These simple findings together with the relative importance of their magnitude have motivated the development of methods that model the dose from scattered particles by means of an extended source integration over the parts visible from the calculation's point view (Ahnesjö *et al* 1992a, Dunscombe and Nieminen 1992, Ahnesjö 1994, Chaney *et al* 1994, Sharpe *et al* 1995, Liu *et al* 1997d) (see figure 14).

9.2.2. Wedge and compensator scatter. Second to structures closest to the target, hard wedges or compensating filters are the most important scatter sources in clinical beams. Analytical calculation models based on first scatter integration over the scattering device (Ahnesjö *et al* 1995, Islam and Van Dyk 1995), and an 'extended phantom concept' using precalculated modulator kernels superimposed over the modulator within the calculation point of view of (Liu *et al* 1997c), have all shown good results.

9.2.3. Collimator scatter. A model for explicit modelling of scatter from the collimators has been presented by Ahnesjö (1995). The model is based on kernels representing the relative energy fluence of photons scattered off a collimator block per unit block length. The kernels can then be applied to the current field of calculation and integrated around the collimating periphery to yield the total collimator scatter energy fluence at the point of calculation. The results show that in most cases scatter from the movable collimators contributes of the order of approximately 1% to the total dose and hence is relatively insignificant. Exceptions yielding larger contributions were found to be for collimators very close to the source, i.e. the primary collimator, and for geometries involving many layered collimators since each upstream side of a collimator block acts as an inlet for photons to be scattered. For direct Monte Carlo simulations, collimator scatter is a low probability event resulting in poor statistics unless special variance reduction techniques are used. As a consequence of the low amount of collimator scatter in photon beams, the term 'collimator scatter factor' should be avoided in favour of 'output factor in air' or '(treatment) head scatter factor'.

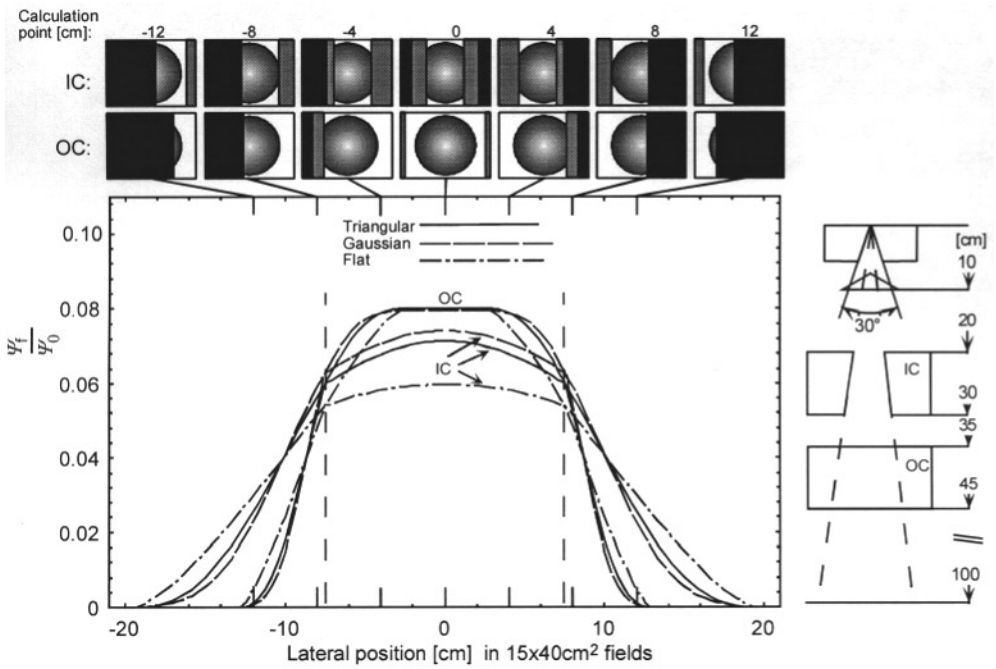

Figure 14. Flattening filter scatter profiles (normalized to the isocentre primary energy fluence Ψ_0) at the isocentre plane for two 15×40 cm^2 fields defined by the inner (IC) and outer (OC) collimators. The profiles are along the 15 cm axis; the machine geometry is shown to the right. The calculation point's eye view of the filter at various positions is shown on top of the chart. Three different distributions of scatter release from the filter are compared; a triangular, a Gaussian and a flat (constant) distribution, all normalized to yield 8% scatter at isocentre when the entire filter is viewed. (From Ahnesjö 1994.)

9.2.4. Monitor backscatter. The problem of backscatter to the monitor from the upper side of a collimator has been studied by a variety of methods. Kubo (1989) used a telescopic technique to exclude the scattered components from the readout of an external detector and measured the variation in monitor units delivered per unit external signal. For a Clinac 1800 he found small variations in the order of 1% to 2% but for a Therac 20 machine the backscatter variation was as high as 7.5% between a 2×2 cm^2 field and 40×40 cm^2 field. Hounsell (1998) also used a telescopic technique and found small variations of the order of less than 1% for an Elekta-Philips SL15 with a protection sheet (3 mm Al) in place between the collimators and the monitor chamber. Hounsell found considerably higher variation when the protection sheet was removed, approximately 5% between a 4×4 cm^2 and 40×40 cm^2 field. Sharpe *et al* (1995), Yu *et al* (1996) and Liu *et al* (1997b) used the number of linac pulses as independent measure of the primary fluence. Liu *et al* used BEAM/EGS4 to perform Monte Carlo simulations of the phenomenon, and found that the monitor backscatter signal varied between 2% and 5% for the largest and smallest fields with a kapton window monitor chamber. When a protection sheet of aluminium was set in place to stop low-energy charged particles the variation reduced to 0.5–1.0%. Yu *et al* applied the technique to a Varian Clinac 600 C and 2100C and found a variation of approximately 2% for the upper jaws and 1% for the lower pair of jaws at energies above 15 MV and about half those values for 6 MV. Lam *et al* (1998) measured the target charge needed to deliver a given amount of monitor units as a function of collimator setting,

as it was considered more reliable than the number of linac pulses. On a Varian Clinac 2100C they found a 2.4% variation for the upper jaws and 1.0% variation for the lower pair of jaws.

A calculation model has been developed by Ahnesjö *et al* (1992a) assuming that the backscatter to direct particles signal ratio (cf equations (3)–(6)) can be determined by a proportionality factor k_b times a geometry factor for diffuse radiation, such that

$$\frac{M_b}{M_0} = k_b \frac{z_{\mathrm{SMD}}^2}{z_{\mathrm{SCD}}^2} \iint_{A_{\mathrm{irr}}} \frac{\cos^3 \theta_A}{\pi z_{\mathrm{MCD}}^2} \, \mathrm{d}A \tag{41}$$

where z_{SMD} is the source to monitor distance, z_{SCD} is the distance from the source to the backscattering collimator surface, z_{MCD} is the monitor to backscattering surface distance, θ_A is the angle between the normal of the backscattering element dA and its view vector of the monitor and A_{irr} is the irradiated backscattering area (in the original paper the source to isocentre distance was erroneously used instead of z_{SMD} and the reflected radiation stated to be isotropic rather than diffuse). A comparison of data from the work by Lam *et al* (1998) with equation (41) yields k_b values of the order of 0.3 to 0.4 for kapton windowed chambers and approximately zero for chambers with metal sheet windows.

9.2.5. Charged particle contamination. Charged particle contamination refers to electrons released within the accelerator treatment head and in the air between the treatment head and the patient. These contribute significantly to the dose in the buildup region. The main sources of origin are (a) electrons released in traversed elements like the flattening filter, wedge etc, (b) the collimators and (c) the air. The higher the beam energy, the more dominant is the first category while air released electrons dominates at lower energies (Beauvais *et al* 1993). The lateral distribution of contaminant electrons has been modelled by a Gaussian pencil beam distribution (Nilsson and Brahme 1979, 1986, Nilsson 1985) whereas the depth dependence has been described by an exponential (Mackie 1984, Beauvais *et al* 1993, Sjögren and Karlsson 1996, Zhu and Palta 1998). Combining the Gaussian lateral dependency with the exponential depth dependency, Ahnesjö and Andreo (1989) determined the Gaussian width, the exponential attenuation and a proportionality factor from depth dose measurements by comparing with Monte Carlo generated 'clean' depth doses without electron contamination (cf section 9.1.1). The resulting parameters were used to define a pencil kernel for direct use in treatment planning (Ahnesjö *et al* 1992b).

At higher beam energies the electron contamination depth dose dependence shows a significant build up (Brahme 1987), deviating from the pure exponential commonly used. Refined measurements at lower energies have revealed a similar structure as shown by Jursinic and Mackie (1996), and they proposed the use of a biexponential function to fit all energies. Although several workers have studied the influence from different materials and their locations in the beam path (McKenna *et al* 1995, Sjögren and Karlsson 1996), no parametrized model general enough to handle all common situations has been proposed so far.

9.3. Implementation concepts

Modelling of the beam transport through the linac head is at least as complicated as modelling the transport in the patient. Hence, considerable computer time has to be spent on 'pre-patient' beam transport which is most efficiently done separately to avoid redundant calculations (several patient voxels are covered by the same beam pixel). Saxner *et al* (1997) used two energy fluence matrices, one to represent the primary beam and one to represent the head scatter fluence, thus allowing for different divergence of respective components. The head

scatter matrix was determined by integration over the scattering elements described by semi-analytical parametrizations. The scattering was treated as extended sources delineated in the calculation point of view up through the collimators (Löfgren 1998). The Peregrine project (Cox *et al* 1997) used Monte Carlo to create an output phase space file in which the position, energy and direction of the exiting particles are scored in a reference plane. The phase space file was then sampled to yield particles for further (Monte Carlo) transport in the patient. The sampling could be biased to reflect a repositioning of a collimator or similar change in the linac head geometry. For sampling efficiency, the particles were grouped into distributions depending on their origin. Liu *et al* (1997a), used a somewhat different approach for wedges and compensators. In their work, these were included within an extended phantom (as part of the patient) and their scatter contributions were predicted using kernel scaling.

10. Inverse techniques

The objective of treatment planning is to find a patient-specific optimal treatment plan that balances cure and risk for complications. It is imperative to include tools for optimization into treatment planning systems to automate the search for optimal treatments (see reviews by Brahme (1995) and Webb (1993, 1997)). Optimization of treatment plans is often referred to as 'inverse planning' since the process would start with defining treatment objectives and let the computer shape the beam set-up. Most present approaches for optimization rely on iterative searches that recomputes the dose with straight 'forward' dose calculations as reviewed above but several authors have published work that treat the dose calculation problem as an inverse problem. We will briefly review these here and also include a section on the problem to reconstruct the dose to a patient given an exit portal dose image.

10.1. Dose optimization as an inverse problem

In the early work by Brahme *et al* the shape of the lateral dose profile of a rotational x-ray beam producing a uniform, circularly symmetric dose distribution in a cylindrical phantom was expressed as a simple analytical function (Brahme *et al* 1982, Lax and Brahme 1982, Cormack and Cormack 1987, Cormack 1987). Later, a general integral equation over the irradiated volume V was expressed to illustrate the degrees of freedom in optimization (Brahme 1995):

$$D(\boldsymbol{r}) = \oiiint_V \iiint h(E, \Omega, \boldsymbol{r}, \boldsymbol{s})\, f_{E,\Omega}(\boldsymbol{s})\, \mathrm{d}E\, \mathrm{d}^2\Omega\, \mathrm{d}^3 s \tag{42}$$

where $\boldsymbol{s}$ denotes the position of the kernel centre, h is a problem-specific energy deposition kernel, f a kernel density function, E the energy of the incident particle and Ω the direction of incidence. For a stationary and monoenergetic beam the above equation (24) simplifies into equation (24) where terma is the kernel density function. The idea of inverse methods for dose calculation was to design a single kernel for several beams and find direct numerical solutions to equation (42). This approach implied pre-assumptions of the beam set-up to include rotations, etc, into a problem-specific rather than radiation quality-specific kernel. One approach has been to use rotational kernels generated from rotated pencil kernels in a cylindrical phantom (Eklöf *et al* 1990, Desobry *et al* 1991). An alternative kernel definition was proposed by Holmes *et al* (1991) where the kernel was the result of photons interacting at a point-of-convergence from a number of directions, calculated as a weighted superposition of rotated monodirectional point kernels. The kernel density is typically calculated by some iterative deconvolution technique including positivity operators to avoid negative kernel density. Incident beam profiles may then be determined through backprojection analogous to image backprojection in computed tomography.

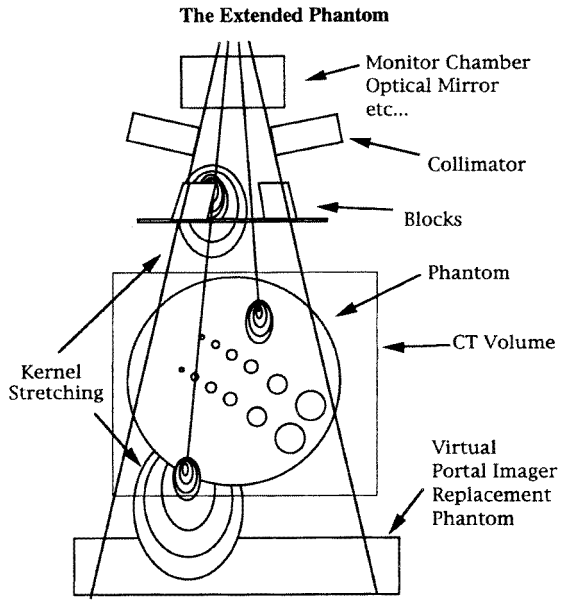

Figure 15. The 'extended phantom' used to compute the dose to a portal imager phantom. (From McNutt *et al* (1996b), with permission.)

The major limitation of the purely inverse approach is that the desired dose distribution is generally not obtainable due to the positivity requirement. Hence, more recent optimization research applies iterations using forward dose calculations (Gustafsson *et al* 1995, Mohan *et al* 1996) and focuses on objective function design (Källman *et al* 1992a, Bortfeld *et al* 1997) and also inclusion of set-up and delivery uncertainties (Löf *et al* 1998, Yan *et al* 1998).

10.2. Dose reconstruction from portal images

Portal dose images (PDIs) contain geometric and dosimetric information useful for treatment verification. Use of portal imaging is a rapidly growing area and we will restrict ourselves to applications of relevance to dose calculations. Transmission dosimetry, as it was originally called by Wong *et al* (1990), refers to the calculation of dose at the portal image plane. The concept is clearly illustrated in the work by McNutt *et al* (1996a, b) where they used an extended phantom concept (see figure 15) to let the portal imager constitute part of the irradiation geometry in a superposition dose calculation algorithm. The radiation transport physics governs the relations between the beam, the patient, the patient dose and the portal image dose thus providing a variety of possibilities to construct verification procedures based on consistency checks of calculated and measured entities.

Ying *et al* (1990) used the entrance fluence matrix and proposed an iterative method where the CT data were corrected to yield portal dose images matching measured images. McNutt *et al* (1996b) assumed, for tomotherapy applications (Mackie *et al* 1993), that the CT density matrix used in the portal dose calculation equals the one used during treatment and proposed to use the technique for dose verification. An alternative to tomotherapy to acquire a representative CT would be megavoltage CT acquisition during treatment (Swindell *et al* 1983, Brahme *et al* 1987, Lewis *et al* 1992).

Hansen *et al* (1996) on the other hand, chose to perform a rigid body transform on the planning CT density map of the patient which assumes that the patient anatomy is unchanged between planning and treatment except for an overall rotation and/or translation. This transform is performed by an operator which is obtained from matching a number of electronic portal images to their corresponding digitally reconstructed radiographs. The dose reconstruction model by Hansen *et al*, unlike the work by McNutt *et al*, relies on a pencil beam kernel convolution algorithm and uses a different normalization approach to access the primary photon fluence level.

Information from an electronic portal imaging device (EPID) in conjunction with a convolution type dose calculation model has also been used to calculate patient exit surface dose distributions (Boellaard *et al* 1997). The primary dose at the imaging device, as extracted from a measured transmission dose, is projected to the exit surface of the patient. From this, the exit scatter dose is determined by convolving the primary dose with an exit dose spread function, which describes the lateral distribution of the scatter exit dose resulting from a pencil beam. The method has been applied to phantoms of variable thickness with the aid of a measured, field size-independent, renormalization correction that takes into account the variation of the scatter dose with phantom thickness. The estimation of exit dose, as the sum of primary and scatter exit doses, in this manner, works well for homogeneous media. The method, however, is probably limited in heterogeneous media mainly because the lateral extent and position of heterogeneity is not taken into account.

11. Conclusions

The need for general dose calculations has long been an issue, since treatment machines are engineered for delivery of complex treatment techniques envisaged to improve treatment results. The motivation for high dose accuracy is the steep dose response of tissues in combination with narrow therapeutic windows. The price–performance relationship for computer systems has not until recently enabled the dose calculation problem to be treated from a first-principle point. Still the most fundamental method, direct particle transport by Monte Carlo simulations is too slow to be practical in routine planning. This can be circumvented by use of parallel hardware but the additional complexity and cost is probably not justified since the point kernel models (with related beam characterization models) fulfil reasonable accuracy requirements. Monte Carlo is, however, firmly established as a necessary tool for providing basic and benchmarking data for faster methods, both for patient dose calculations and for treatment machine characterization. The consistency between experimental methods, Monte Carlo generated phase space distributions and semianalytical methods for beam characterization is an important area for further research. For routine use, point kernel models are well examined and are also conceptually simple, which is important for the understanding of dose results. Charged particle disequilibrium, a long-standing issue for lung dose calculations, is modelled by point kernel models but there is a residual error caused by the rectilinear density scaling approach. Better scaling methods have been proposed but are still premature. Pencil kernel models share the features of point kernel models with respect to beam modulations but have the same limitations as classical broad beam models with respect to the impact from heterogeneities. Pencil kernel models are, however, faster and simpler to use than point kernel models and will therefore be used for the foreseeable future as part of the optimization algorithms for finding optimal beam modulations and field shapes. Electron contamination is not addressed by the basic photon kernel models and treatment planning implementations have to rely on separate models which at present are less well developed than the pure photon models. This weakness is generally bypassed by choosing calibration procedures utilizing depth greater than the maximum depth of contamination influence.

The increased complexity encountered in 3D conformal therapy implies an increased dependency on monitor unit calculations provided by the treatment planning systems. Implementation errors, modelling limitations and flaws in system handling and data logistics make independent checks of monitor unit calculations imperative. These should be simple to implement and rely on independently measured data. Suitable candidates for such models are scatter integration and scaling techniques, as reviewed in sections 5.2.1 and 5.2.2, combined with 1D depth scalings for heterogeneities. A general problem with empirical scatter scaling techniques is that they are developed for open, not modulated beams, and there is a great need to improve these models to include effects from modulations. Pencil kernel models will probably provide the link between empirical results and first principle models in the search for such methods. The need for quality assurance of complex treatment delivery has boosted an interest in electronic portal imaging. Several computation models have the potential to calculate the dose also to an imager, thus providing additional tools for dosimetric verification.

The level of accuracy achieved by any kind of model is subject to implementation details which should be clearly outlined by the manufacturers of treatment planning systems. The quality assurance of treatment related data is a tedious task requiring a cooperative attitude across organizational borders. In the end, no dose results can be better than the model approximations and the quality of data fed into the model.

Acknowledgments

The detailed and constructive criticism provided by the Board Members is gratefully acknowledged.

References

Ågren-Cronqvist A-K 1995 Quantification of the response of heterogeneous tumours and organized normal tissues to fractionated radiotherapy *PhD Thesis* University of Stockholm

Ahnesjö A 1984 Application of transform algorithms for calculation of absorbed dose in photon beams *Int. Conf. on the Use of Computers in Radiation Therapy, VIII ICCR (Toronto, Canada)* (Los Alamos, CA: IEEE Computer Society Press) pp 17–20

——1987 Invariance of convolution kernels applied to dose calculations for photon beams *Int. Conf. on the Use of Computers in Radiation Therapy, IX ICCR (Scheveningen, The Netherlands)* ed I A D Bruinvis, P H van der Giessen, H J van Kleffens and F W Wittkämper (Amsterdam: Elsevier) pp 99–102

——1989 Collapsed cone convolution of radiant energy for photon dose calculation in heterogeneous media *Med. Phys.* **16** 577–92

——1991 Dose calculation methods in photon beam therapy using energy deposition kernels *PhD Thesis* University of Stockholm

——1992 Dose calculation methods for multidimensional treatment planning *Three-Dimensional Treatment Planning (Geneva)* ed P Minet (Liège: European Association of Radiology) pp 277–88

——1994 Analytic modeling of photon scatter from flattening filters in photon therapy beams *Med. Phys.* **21** 1227–35

——1995 Collimator scatter in photon therapy beams *Med. Phys.* **22** 267–78

——1997 Cone discretization for the collapsed cone algorithm *Int. Conf. on the Use of Computers in Radiation Therapy, XII ICCR (Salt Lake City, Utah, USA)* ed D D Leavitt and G Starkschall (Madison, WI: Medical Physics Publishing) pp 114–16

Ahnesjö A and Andreo P 1989 Determination of effective bremsstrahlung spectra and electron contamination for photon dose calculations *Phys. Med. Biol.* **34** 1451–64

Ahnesjö A, Andreo P and Brahme A 1987 Calculation and application of point spread functions for treatment planning with high energy photon beams *Acta Oncol.* **26** 49–56

Ahnesjö A, Knöös T and Montelius A 1992a Application of the convolution method for calculation of output factors for therapy photon beams *Med. Phys.* **19** 295–301

Ahnesjö A and Mackie T R 1987 Analytical description of Monte Carlo generated photon dose convolution kernels *Int. Conf. on the Use of Computers in Radiation Therapy, IX ICCR (Scheveningen, The Netherlands)* ed I A D Bruinvis, P H van der Giessen, H J van Kleffens and F W Wittkämper (Amsterdam: Elsevier) pp 197–200

Ahnesjö A, Saxner M and Trepp A 1992b A pencil beam model for photon dose calculation *Med. Phys.* **19** 263–73

Ahnesjö A and Trepp A 1991 Acquisition of the effective lateral energy fluence distribution for photon beam dose calculations by convolution models *Phys. Med. Biol.* **36** 973–85

Ahnesjö A, Weber L and Nilsson P 1995 Modeling transmission and scatter for photon beam attenuators *Med. Phys.* **22** 1711–20

Alcouffe R E, Baker R S, Brinkley F W, Marr D R, O'Dell R D and Walters W F 1995 DANTSYS: a diffusion accelerated neutral particle transport code system *Report* LA-12969-M UC-705 (Los Alamos National Laboratory)

Andreo P 1990 Uncertainties in dosimetric data and beam calibration *Int. J. Radiat. Oncol. Biol. Phys.* **19** 1233–47

——1991 Monte Carlo techniques in medical radiation physics *Phys. Med. Biol.* **36** 861–920

Andreo P and Brahme A 1984 Restricted energy loss straggling and multiple scattering of electrons in mixed Monte Carlo procedures *Radiat. Res.* **100** 16–29

Archer B R, Almond P R and Wagner L K 1985 Application of a Laplace transform pair model for high-energy x-ray spectral reconstruction *Med. Phys.* **12** 630–3

Åsell M 1999 Development of optimized radiation therapy using external electron and photon beams *PhD Thesis* University of Stockholm

Aspradakis M M 1996 A study to assess and improve dose computations in photon beam therapy *PhD Thesis* University of Edinburgh

Aspradakis M M and Redpath A T 1997 A technique for the fast calculation of three-dimensional photon dose distributions using the superposition model. *Phys. Med. Biol.* **42** 1475–89

Attix F A 1986 *Introduction to Radiological Physics and Radiation Dosimetry* (New York: Wiley)

Austin-Seymour M, Chen G T Y, Rosenman J, Michalski J, Lindsley K and Goitein M 1995 Tumor and target delineation: current research and future challenges *Int. J. Radiat. Oncol. Biol. Phys.* **33** 1041–52

Baker C R, Amaée B and Spyrou N M 1995 Reconstruction of megavoltage photon spectra by attenuation analysis *Phys. Med. Biol.* **40** 529–42

Baker C R and Peck K K 1997 Reconstruction of 6 MV photon spectra from measured transmission including maximum energy estimation *Phys. Med. Biol.* **42** 2041–51

Batho H F 1964 Lung corrections in cobalt 60 beam therapy *J. Can. Assoc. Radiol.* **15** 79–83

Battista J J and Sharpe M B 1992 True three-dimensional dose computations for megavoltage x-ray therapy: a role for the superposition principle *Australas. Phys. Eng. Sci. Med.* **15** 159–78

Beaudoin L 1968 Analytical approach to the solution of the dosimetry in heterogeneous media *MSc Thesis* University of Toronto

Beauvais H, Bridier A and Dutreix A 1993 Characteristics of contamination electrons in high energy photon beams *Radiother. Oncol.* **29** 308–16

Bell G I and Glasstone S 1970 *Nuclear Reactor Theory* (Malabar, FL: Krieger)

Bellman R and Wing G M 1975 *An Introduction to Invariant Imbedding* (New York: Wiley)

Berger M J 1963 Monte Carlo calculation of the penetration and diffusion of fast charged particles *Methods in Computational Physics* vol 1, ed B Alder, S Fernbach and M Rotenberg (New York: Academic) pp 135–215

Bielajew A F and Rogers D W O 1987 PRESTA: The parameter reduced electron-step transport algorithm for electron Monte Carlo transport *Nucl. Instrum. Methods* B **18** 165–81

BJR 1983 Central axis depth dose data for use in radiotherapy *Br. J. Radiol.* (suppl 17)

——1996 Central axis depth dose data for use in radiotherapy *Br. J. Radiol.* (suppl 25)

Bjärngard B E 1987 On Fano's and O'Connor's theorems *Radiat. Res.* **109** 184–9

Bjärngard B E and Cunningham J R 1986 Comments on 'Validity of the concept of separating primary and scatter dose' (letter) *Med. Phys.* **13** 760–1

Bjärngard B E and Petti P L 1988 Description of the scatter component in photon-beam data *Phys. Med. Biol.* **33** 21–32

Bjärngard B E and Shackford H 1994 Attenuation in high-energy x-ray beams *Med. Phys.* **21** 1069–73

Bjärngard B E and Siddon R L 1982 A note on equivalent circles, squares, and rectangles *Med. Phys.* **9** 258–60

Bjärngard B E, Tsai J S and Rice R K 1989 Attenuation in very narrow photon beams *Radiat. Res.* **118** 195–200

——1990 Doses on the central axes of narrow 6-MV x-ray beams *Med. Phys.* **17** 794–9

Bjärngard B E and Vadash P 1995 Analysis of central-axis doses for high-energy x-rays *Med. Phys.* **22** 1191–5

Bjärngard B E, Vadash P and Ceberg C P 1997 Quality control of measured x-ray beam data *Med. Phys.* **24** 1441–4

Bloch P and Altschuler M D 1995 Three-dimensional photon beam calculations *Radiation Therapy Physics* ed A Smith (Berlin: Springer)

Boellaard B E, van Herk M and Mijnheer B J 1997 A convolution model to convert transmission dose images to exit dose distributions *Med. Phys.* **24** 189–99

Börgers C 1998 Complexity of Monte Carlo and deterministic dose-calculation methods *Phys. Med. Biol.* **43** 517–28

Bortfeld T, Boyer A L, Schlegel W, Kahler D L and Waldron T J 1994 Realization and verification of three-dimensional conformal radiotherapy with modulated fields *Int. J. Radiat. Oncol. Biol. Phys.* **30** 899–908

Bortfeld T, Schlegel W and Rhein B 1993 Decomposition of pencil beam kernels for fast dose calculations in three-dimensional treatment planning *Med. Phys.* **20** 311–18

Bortfeld T, Stein J and Preiser K 1997 Clinically relevant intensity modulation optimization using physical criteria *Int. Conf. on the Use of Computers in Radiation Therapy, XII ICCR (Salt Lake City, Utah, USA)* ed D D Leavitt and G Starkschall (Madison, WI: Medical Physics Publishing) pp 1–4

Bourland J D and Chaney E L 1992 A finite-size pencil beam model for photon dose calculations in three dimensions *Med. Phys.* **19** 1401–12

Boyer A L 1988 Relationship between attenuation coefficients and dose-spread kernels *Radiat. Res.* **113** 235–42

Boyer A L and Mok E C 1984 Photon beam modeling using Fourier transform techniques *Int. Conf. on the Use of Computers in Radiation Therapy, VIII ICCR (Toronto, Canada)* (Los Alamos, CA: IEEE Computer Society Press) pp 14–16

——1985 A photon dose distribution model employing convolution calculations *Med. Phys.* **12** 169–77

——1986 Calculation of photon dose distributions in an inhomogeneous medium using convolutions *Med. Phys.* **13** 503–9

Boyer A L and Schultheiss T 1988 Effects of dosimetric and clinical uncertainty on complication-free local tumor control *Radiother. Oncol.* **11** 65–71

Boyer A L, Zhu Y, Wang L and Francois P 1989 Fast Fourier transform convolution calculations of x-ray isodose distributions in homogeneous media *Med. Phys.* **16** 248–53

Brahme A 1977 Restricted mass energy absorption coefficients for use in dosimetry *Internal Report* SSI:1977-009 (National Institute of Radiation Protection)

——1984 Dosimetric precision requirements in radiation therapy *Acta Radiol. Oncol.* **23** 379–91

——1987 Design principles and clinical possibilities with a new generation of radiation therapy equipment. A review *Acta Oncol.* **26** 403–12

——(ed) 1988 Accuracy requirements and quality assurance of external beam therapy with photons and electrons *Acta Radiol. Oncol.* (suppl 1)

——1995 Treatment optimization using physical and radiobiological objective functions *Radiation Therapy Physics* ed A Smith (Berlin: Springer)

Brahme A, Lind B and Nafstadius P 1987 Radiotherapeutic computed tomography with scanned photon beams *Int. J. Radiat. Oncol. Biol. Phys.* **13** 95–101

Brahme A, Roos J E and Lax I 1982 Solution of an integral equation encountered in rotation therapy *Phys. Med. Biol.* **27** 1221–9

Briesmeister J F 1988 MCNP—A general Monte Carlo *N*-particle transport code *Report* LA-12625-M (Los Alamos National Laboratory)

Cassell K J, Hobday P A and Parker R P 1981 The implementation of a generalised Batho inhomogeneity correction for radiotherapy planning with direct use of CT numbers *Phys. Med. Biol.* **26** 825–33

Ceberg C P, Bjärngard B E and Zhu T C 1996 Experimental determination of the dose kernel in high-energy x-ray beams *Med. Phys.* **23** 505–11

Chaney E L, Cullip T J and Gabriel T A 1994 A Monte Carlo study of accelerator head scatter *Med. Phys.* **21** 1383–90

Chin L M, Kijewski P K, Svensson G K and Bjärngard B E 1983 Dose optimization with computer-controlled gantry rotation, collimator motion and dose-rate variation *Int. J. Radiat. Oncol. Biol. Phys.* **9** 723–9

Chui C and Mohan R 1984 Differential pencil beam dose computation model (abstract) *Med. Phys.* **11** 392

Chui C S, LoSasso T and Spirou S 1994 Dose calculation for photon beams with intensity modulation generated by dynamic jaw or multileaf collimations *Med. Phys.* **21** 1237–44

Clarkson J R 1941 A note on depth doses in fields of irregular shape *Br. J. Radiol.* **14** 265–8

Convery D J and Rosenbloom M E 1992 The generation of intensity-modulated fields for conformal radiotherapy by dynamic collimation *Phys. Med. Biol.* **37** 1359–74

Cormack A M 1987 A problem in rotation therapy with X-rays *Int. J. Radiat. Oncol. Biol. Phys.* **13** 623–30

Cormack A M and Cormack R A 1987 A problem in rotation therapy with X-rays: dose distributions with an axis of symmetry *Int. J. Radiat. Oncol. Biol. Phys.* **13** 1921–5

Cox L J, Schach von Wittenau A E, Bergstrom P M J, Mohan R, Libby B, Wu Q and Lovelock D M J 1997 Photon beam description in PEREGRINE for Monte Carlo dose calculations *Int. Conf. on the Use of Computers in Radiation Therapy, XII ICCR (Salt Lake City, Utah, USA)* ed D D Leavitt and G Starkschall (Madison, WI: Medical Physics Publishing) pp 142–5

Cunningham J R 1972 Scatter-air ratios *Phys. Med. Biol.* **17** 42–51

Cunningham J R 1983 Current and future developement of tissue inhomogeneity corrections for photon beam clinical dosimetry with the use of CT *Computed Tomography in Radiation Therapy* ed C C Ling, C C Rogers and R J Morton (New York: Raven Press) pp 209–18

Cunningham J R and Beaudoin L 1973 Calculations for tissue inhomogeneities with experimental verification *XIII Int. Congress of Radiology (Madrid)* XIII, pp 653–7

Cunningham J R, Shrivastava P N and Wilkinson J M 1972 Program IRREG-calculation of dose from irregularly shaped radiation beams *Comput. Programs Biomed.* **2** 192–9

Dahlin H, Lamm I-L, Landberg T, Levernes S and Ulsø N 1983 User requirements on CT-based computed dose planning systems in radiation therapy *Acta Radiol. Oncol.* **22** 398–414

Dasu A and Denekamp J 1999 Superfractionation as a potential hypoxic cell radiosensitizer: prediction of an optimum dose per fraction *Int. J. Radiat. Oncol. Biol. Phys.* **43** 1083–94

Day M J 1950 A note on the calculation of dose in x-ray fields *Br. J. Radiol.* **23** 368–9

——1972 The equivalent field method for axial dose determinations in rectangular fields *Br. J. Radiol.* (suppl 10)

——1978 The equivalent field method for axial dose determinations in rectangular fields *Br. J. Radiol.* (suppl 11) 95–100

——1983 The normalised peak scatter factor and normalised scatter functions for high energy photon beams *Br. J. Radiol.* (suppl 17) 131–6

Day M J and Aird E G A 1996 The equivalent field method for dose determination in rectangular fields *Br. J. Radiol.* (suppl 25) 138–51

Dean R D 1980 A scattering kernel for use in true three-dimensional dose calculations (abstract) *Med. Phys.* **7** 429

DeMarco J J, Solberg T D and Smathers J B 1998 A CT-based Monte Carlo simulation tool for dosimetry planning and analysis *Med. Phys.* **25** 1–11

Desobry G E and Boyer A L 1991 Bremsstrahlung review: an analysis of the Schiff spectrum *Med. Phys.* **18** 497–505

——1994 An analytic calculation of the energy fluence spectrum of a linear accelerator *Med. Phys.* **21** 1943–52

Desobry G E, Wells N H and Boyer A L 1991 Rotational kernels for conformal therapy *Med. Phys.* **18** 481–7

Difilippo F C 1998 Forward and adjoint methods for radiotherapy planning *Med. Phys.* **25** 1702–10

Dische S, Saunders M I, Williams C, Hopkins A and Aird E 1993 Precision in reporting the dose given in a course of radiotherapy *Radiother. Oncol.* **29** 287–93

Dunscombe P B and Nieminen J M 1992 On the field-size dependence of relative output from a linear accelerator *Med. Phys.* **19** 1441–4

Dutreix A, Bjärngard B E, Bridier A, Mijnheer B, Shaw J E and Svensson H 1997 Monitor unit calculation for high energy photon beams *Physics for Clinical Radiotherapy, Booklet No. 3* (Leuven/Apeldoorn: Garant)

Dutreix J, Dutreix A and Tubiana M 1965 Electronic equilibrium and transition stages *Phys. Med. Biol.* **10** 177–90

Ebert M A, Hoban P W and Keall P J 1996 Modelling clinical accelerator beams: a review *Australas. Phys. Eng. Sci. Med.* **19** 131–50

Eklöf A, Ahnesjö A and Brahme A 1990 Photon beam energy deposition kernels for inverse radiotherapy planning *Acta Oncol.* **29** 447–54

El-Khatib E and Battista J J 1984 Improved lung dose calculation using tissue-maximum ratios in the Batho correction *Med. Phys.* **11** 279–86

Faddegon B A, Ross C K and Rogers D W O 1990 Forward-directed bremsstrahlung of 10- to 30-MeV electrons incident on thick targets of Al and Pb *Med. Phys.* **17** 773–85

——1991 Angular distribution of bremsstrahlung from 15-MeV electrons incident on thick targets of Be, Al, and Pb *Med. Phys.* **18** 727–39

Fano U 1954 Note on the Bragg-Gray cavity principle for measuring energy dissipation *Radiat. Res.* **1** 237–40

Fraass B, Doppke K, Hunt M, Kutcher G, Starkschall G, Stern R and Van Dyke J 1998 American Association of Physicists in Medicine Radiation Therapy Committee Task Group 53: quality assurance for clinical radiotherapy treatment planning *Med. Phys.* **25** 1773–829

Fraass B A 1995 The development of conformal radiation therapy *Med. Phys.* **22** 1911–21

Francois P, Coste F, Bonnet J and Caselles O 1997 Validation of reconstructed bremsstrahlung spectra between 6 MV and 25 MV from measured transmission data *Med. Phys.* **24** 769–73

Goitein M and Abrams M 1983 Multi-dimensional treatment planning: I. Delineation of anatomy *Int. J. Radiat. Oncol. Biol. Phys.* **9** 777–87

Goitein M, Abrams M, Rowell D, Pollari H and Wiles J 1983 Multi-dimensional treatment planning: II. Beam's eye-view, back projection, and projection through CT sections *Int. J. Radiat. Oncol. Biol. Phys.* **9** 789–97

Gokhale P, Hussein E M A and Kulkarni N 1994 Determination of beam orientation in radiotherapy planning *Med. Phys.* **21** 393–400

Greene D and Stewart J R 1965 Isodose curves in non-uniform phantoms *Br. J. Radiol.* **38** 378–85

Gupta S K and Cunningham J R 1966 Measurement of tissue-air ratios and scatter functions for large field sizes, for cobalt 60 gamma radiation *Br. J. Radiol.* **39** 7–11

Gustafsson A 1996 Development of a versatile algorithm for optimization of radiation therapy *PhD Thesis* University of Stockholm

Gustafsson A, Lind B K and Brahme A 1994 A generalized pencil beam algorithm for optimization of radiation therapy *Med. Phys.* **21** 343–56

Gustafsson A, Lind B K, Svensson R and Brahme A 1995 Simultaneous optimization of dynamic multileaf collimation and scanning patterns or compensation filters using a generalized pencil beam algorithm *Med. Phys.* **22** 1141–56

Hannallah D, Zhu T C and Bjärngard B E 1996 Electron disequilibrium in high-energy x-ray beams *Med. Phys.* **23** 1867–71

Hansen V N, Evans P M and Swindell W 1996 The application of transit dosimetry to precision radiotherapy *Med. Phys.* **23** 713–21

Harder D 1974 Fano's theorem and the multiple scattering correction. *Fourth Symp. on Microdosimetry (Verbania-Pallanza, Italy)* ed J Booz, H G Ebert, R Eickel and A Waker (Luxembourg: Commission of the European Communities) pp 677–93

Harms W B, Low D A, Wong J W and Purdy J A 1998 A software tool for the quantitative evaluation of 3D dose calculation algorithms *Med. Phys.* **25** 1830–36

Hartmann Siantar C L, Bergstrom P M, Chandler W P, Chase L, Cox L J, Daly T P, Garrett D, Hornstein S M, House R K, Moses E I, Patterson R W, Rathkopf J A and Schach von Wittenau A E 1997 Lawrence Livermore National Laboratory's PEREGRINE project *Int. Conf. on the Use of Computers in Radiation Therapy, XII ICCR (Salt Lake City, Utah, USA)* ed D D Leavitt and G Starkschall (Madison, WI: Medical Physics Publishing) pp 19–22

Heukelom S, Lanson J H and Mijnheer B J 1994 Wedge factor constituents of high energy photon beams: field size and depth dependence *Radiother. Oncol.* **30** 66–73

——1997 Differences in wedge factor determination in air using a PMMA mini-phantom or a brass buildup cap *Med. Phys.* **24** 1986–91

Hoban P W 1995 Accounting for the variation in collision kerma-to-terma ratio in polyenergetic photon beam convolution *Med. Phys.* **22** 2035–44

Hoban P W, Murray D C and Round W H 1994 Photon beam convolution using polyenergetic energy deposition kernels *Phys. Med. Biol.* **39** 669–85

Holmes T, Mackie T R, Simpkin D and Reckwerdt P 1991 A unified approach to the optimization of brachytherapy and external beam dosimetry *Int. J. Radiat. Oncil. Biol. Phys.* **20** 859–73

Holt J G, Laughlin J S and Moroney J P 1970 The extension of the concept of tissue-air ratios (TAR) to high-energy x-ray beams *Radiology* **96** 437–46

Hounsell A R 1998 Monitor chamber backscatter for intensity modulated radiation therapy using multileaf collimators *Phys. Med. Biol.* **43** 445–54

Huang P H, Kase K R and Bjärngard B E 1983 Reconstruction of 4-MV bremsstrahlung spectra from measured transmission data *Med. Phys.* **10** 778–85

Huizenga H and Storchi P R M 1989 Numerical calculation of energy deposition by broad high-energy electron beams *Phys. Med. Biol.* **34** 1371–96

Hurkmans C, Knöös T, Nilsson P, Svahn-Tapper G and Danielsson H 1995 Limitations of a pencil beam approach to photon dose calculations in the head and neck region *Radiother. Oncol.* **37** 74–80

IAEA 1987 Absorbed dose determination in photon and electron beams. An international code of practice *IAEA Technical Report Series* No. 277 (Vienna: International Atomic Energy Agency)

ICCR 1970 Computers in radiotherapy *Int. Conf. on the Use of Computers in Radiation Therapy, III ICCR (Glasgow, Scotland)* ed A S Glicksman, M Cohen and J R Cunningham (British Journal of Radiology)

ICRU 1963 Clinical dosimetry handbook 87 *ICRU Publication* 10d (Washington, DC: National Bureau of Standards)

——1973 Measurement of absorbed dose in a phantom irradiated by a single beam of x or gamma rays *ICRU Publication* 23 (Bethesda, MA: International Commission on Radiation Units and Measurements)

——1976 Determination of absorbed dose in a patient irradiated by beams of x or gamma rays in radiotherapy procedures *ICRU Publication* 24 (Bethesda, MD: International Commission on Radiation Units and Measurements)

——1987 Use of computers in external beam radiotherapy procedures with high-energy photons and electrons *ICRU Publication* 42 (Bethesda, MD: International Commission on Radiation Units and Measurements)

——1998 Fundamental quantities and units for ionizing radiation *ICRU Publication* 60 (Bethesda, MD: International Commission on Radiation Units and Measurements)

Islam M K and Van Dyk J 1995 Effects of scatter generated by beam-modifying absorbers in megavoltage photon beams *Med. Phys.* **22** 2075–81

Iwasaki A 1985 A method of calculating high-energy photon primary absorbed dose in water using forward and backward spread dose-distribution functions *Med. Phys.* **12** 731–7

——1990 Calculation of three-dimensional photon primary absorbed dose using forward and backward spread dose-distribution functions *Med. Phys.* **17** 195–202

Iwasaki A and Ishito T 1984 The differential scatter-air ratio and differential backscatter factor method combined with the density scaling theorem *Med. Phys.* **11** 755–63

Jaffray D A, Battista J J, Fenster A and Munro P 1993 X-ray sources of medical linear accelerators: focal and extra-focal radiation *Med. Phys.* **20** 1417–27

Janssen J J, Korevaar E W, Storchi P R M and Huizenga H 1997 Numerical calculation of energy deposition by high-energy electron beams: III-B. Improvements to the 6D phase space evolution model *Phys. Med. Biol.* **42** 1441–9

Johns H E, Darby E K, Haslam R N, Katz L and Harrington E L 1949 Depth dose data and isodose distributions for radiation from a 22 MeV betatron *Am. J. Roentgenol.* **62** 257–68

Johns H E, Whitmore G F, Watson T A and Umberg F H 1953 A system of dosimetry for rotation therapy and typical rotation distribution *J. Can. Assoc. Radiol.* **4** 1–14

Jung B, Montelius A, Dahlin H, Ekström P, Ahnesjö A, Högström B and Glimelius B 1997 The conceptual design of a radiation oncology planning system *Comput. Methods Prog. Biom.* **52** 79–92

Jursinic P A and Mackie T R 1996 Characteristics of secondary electrons produced by 6, 10 and 24 MV x-ray beams *Phys. Med. Biol.* **41** 1499–509

Karlsson M, Nyström H and Svensson H 1993 Photon beam characteristics on the MM50 racetrack microtron and a new approach for beam quality determination *Med. Phys.* **20** 143–9

Karzmark C J, Deubert A and Loevinger R 1965 Letter to Editor: tissue-phantom ratios—an aid to treatment planning *Br. J. Radiol.* **38** 158–9

Kase K R and Svensson G K 1986 Head scatter data for several linear accelerators (4–18 MV) *Med. Phys.* **13** 530–2

Kawrakow I and Bielajew A F 1998 On the condensed history technique for electron transport *Nucl. Instrum. Methods* B **142** 253–80

Kawrakow I, Fippel M and Friedrich K 1996 3D electron dose calculation using a voxel based Monte Carlo algorithm (VMC) *Med. Phys.* **23** 445–57

Keall P and Hoban P 1995 Accounting for primary electron scatter in x-ray beam convolution calculations *Med. Phys.* **22** 1413–18

——1996a Superposition dose calculation incorporating Monte Carlo generated electron track kernels *Med. Phys.* **23** 479–85

——1996b A review of electron beam dose calculation algorithms *Australas. Phys. Eng. Sci. Med.* **19** 111–30

Keller H, Fix M and Rüegsegger P 1998 Calibration of a portal imaging device for high-precision dosimetry: a Monte Carlo study. *Med. Phys.* **25** 1891–902

Khan F M, Moore V C and Sato S 1972 Depth dose and scatter analysis of 10 MV X rays *Radiology* **102** 165–9

Kijewski P K, Bjärngard B E and Petti P L 1986 Monte Carlo calculations of scatter dose for small field sizes in a ^{60}Co beam *Med. Phys.* **13** 74–7

Kijewski P K, Chin L M and Bjärngard B E 1978 Wedge-shaped dose distributions by computer-controlled collimator motion *Med. Phys.* **5** 426–9

Kim S, Palta J R and Zhu T C 1998 A generalized solution for the calculation of in-air output factors in irregular fields *Med. Phys.* **25** 1692–701

King L V 1912 Absorption problems in radioactivity *Phil. Mag.* **xxiii** 242–50

Knöös T, Ahnesjö A, Nilsson P and Weber L 1995 Limitations of a pencil beam approach to photon dose calculations in lung tissue *Phys. Med. Biol.* **40** 1411–20

Koch H W and Motz J W 1959 Bremsstrahlung cross-section formulas and related data *Rev. Mod. Phys.* **31** 920–55

Kubo H 1989 Telescopic measurements of backscattered radiation from secondary collimator jaws to a beam monitor chamber using a pair of slits *Med. Phys.* **16** 295–8

Küster G, Bortfeld T and Schlegel W 1997 Monte Carlo simulations of radiation beams from radiotherapy units and beam limiting devices using the program GEANT *Int. Conf. on the Use of Computers in Radiation Therapy, XII ICCR (Salt Lake City, Utah, USA)* ed G Starkschall (Madison, WI: Medical Physics Publishing) pp 150–2

Källman P, Ågren A and Brahme A 1992b Tumour and normal tissue responses to fractionated non-uniform dose delivery. *Int. J. Radiat. Biol.* **62** 249–62

Källman P, Lind B K and Brahme A 1992a An algorithm for maximizing the probability of complication-free tumour control in radiation therapy *Phys. Med. Biol.* **37** 871–90

Lam K L, Muthuswamy M S and Ten Haken R K 1998 Measurement of backscatter to the monitor chamber of medical accelerators using target charge *Med. Phys.* **25** 334–8

Larson K B and Prasad S C 1978 Absorbed dose computations for inhomogeneous media in radiation-treatment planning using differential scatter-air ratios *2nd Ann. Symp. on Computer Applications in Medical Care (Washington DC)* (New York: IEEE) pp 93–9

Lax I and Brahme A 1982 Rotation therapy using a novel high-gradient filter *Radiology* **145** 473–8

Lee P C 1997 Monte Carlo simulations of the differential beam hardening effect of a flattening filter on a therapeutic x-ray beam *Med. Phys.* **24** 1485–9

Lewis D G, Swindell W, Morton E J, Evans P M and Xiao Z R 1992 A megavoltage CT scanner for radiotherapy verification *Phys. Med. Biol.* **37** 1985–99

Liu H H, Mackie T R and McCullough E C 1997a Calculating dose and output factors for wedged photon radiotherapy fields using a convolution/superposition method *Med. Phys.* **24** 1714–28

——1997b Calculating output factors for photon beam radiotherapy using a convolution/superposition method based on a dual source photon beam model *Med. Phys.* **24** 1975–85

——1997c Correcting kernel tilting and hardening in convolution/superposition dose calculations for clinical divergent and polychromatic photon beams *Med. Phys.* **24** 1729–41

——1997d A dual source photon beam model used in convolution/superposition dose calculations for clinical megavoltage x-ray beams *Med. Phys.* **24** 1960–74

Liu H H, McCullough E C and Mackie T R 1998 Calculating dose distributions and wedge factors for photon treatment fields with dynamic wedges based on a convolution/superposition method *Med. Phys.* **25** 56–63

Loevinger R 1950 Distribution of absorbed energy around a point source of beta radiation *Science* **112** 530–1

——1956 The dosimetry of beta sources in tissue: the point source function *Radiology* **66** 55–62

Löf J, Lind B K and Brahme A 1998 An adaptive control algorithm for optimization of intensity modulated radiotherapy considering uncertainties in beam profiles, patient set-up and internal organ motion. *Phys. Med. Biol.* **43** 1605–28

Löfgren A 1998 Polygon delineation of thick collimator apertures from arbitrary view points *MSc Thesis* University of Uppsala

Lovelock D M, Chui C S and Mohan R 1995 A Monte Carlo model of photon beams used in radiation therapy *Med. Phys.* **22** 1387–94

Luxton G and Astrahan M A 1988 Output factor constituents of a high-energy photon beam *Med. Phys.* **15** 88–91

Lydon J M 1998 Photon dose calculations in homogeneous media for a treatment planning system using a collapsed cone superposition convolution algorithm *Phys. Med. Biol.* **43** 1813–22

Mackie T R 1984 A study of charged particles and scattered photons in mega-voltage x-ray beams *PhD Thesis* University of Alberta

——1990 Applications of the Monte Carlo method in radiotherapy *The Dosimetry of Ionizing Radiation* vol 3, ed K R Kase, B Bjärngard and F H Attix (New York: Academic) pp 541-620

Mackie T R, Bielajew A F, Rogers D W O and Battista J J 1988 Generation of photon energy deposition kernels using the EGS Monte Carlo code *Phys. Med. Biol.* **33** 1–20

Mackie T R, Holmes T, Swerdloff S, Reckwerdt P, Deasy J O, Yang J, Paliwal B and Kinsella T 1993 Tomotherapy: a new concept for the delivery of dynamic conformal radiotherapy *Med. Phys.* **20** 1709–19

Mackie T R, Reckwerdt P, McNutt T, Gehring M and Sanders C 1996 Photon beam dose computations *Teletherapy: Present and Future* ed J Palta and T R Mackie (College Park, MD: American Association of Physicists in Medicine) pp 103–35

Mackie T R, Reckwerdt P and Papanikolaou N 1995 3-D photon beam dose algorithms *3-D Radiation Treatment Planning and Conformal Therapy* ed J A Purdy and B Emami (Madison, WI: Medical Physics Publishing)

Mackie T R and Scrimger J W 1984 Computing radiation dose for high energy X-rays using a convolution method *Int. Conf. on the Use of Computers in Radiation Therapy, VIII ICCR (Toronto, Canada)* (Los Alamos, CA: IEEE Computer Society Press) pp 36–40

Mackie T R, Scrimger J W and Battista J J 1985 A convolution method of calculating dose for 15-MV x rays *Med. Phys.* **12** 188–96

Manfredotti C, Nastasi U, Marchisio R, Ongaro C, Gervino G, Ragona R, Anglesio S and Sannazzari G 1990 Monte Carlo simulation of dose distribution in electron beam radiotherapy treatment planning *Nucl. Instrum. Methods* A **291** 646–54

Mayneord W V 1945 Energy absorption. IV The mathematical theory of integral dose in radium therapy *Br. J. Radiol.* **18** 12–19

McGary J E and Boyer A L 1997 An interactive, parallel, three-dimensional fast Fourier transform convolution dose calculation using a supercomputer *Med. Phys.* **24** 519–22

McKenna M G, Chen X G, Altschuler M D and Bloch P 1995 Calculation of the dose in the buildup region for high energy photon beam. Treatment planning when beam spoilers are employed *Radiother. Oncol.* **34** 63–8

McLellan J, Papiez L, Sandison G A, Huda W and Therrien P 1992 A numerical method for electron transport calculations *Phys. Med. Biol.* **37** 1109–25

McNutt T R, Mackie T R, Reckwerdt P and Paliwal B R 1996a Modeling dose distributions from portal dose images using the convolution/superposition method *Med. Phys.* **23** 1381–92

McNutt T R, Mackie T R, Reckwerdt P, Papanikolaou N and Paliwal B R 1996b Calculation of portal dose using the convolution/superposition method *Med. Phys.* **23** 527–35

Metcalfe P E, Hoban P W, Murray D C and Round W H 1989 Modelling polychromatic high energy photon beams by superposition *Australas. Phys. Eng. Sci. Med.* **12** 138–48

Metcalfe P E, Hoban P W, Murray D C and Round W H 1990 Beam hardening of 10 MV radiotherapy x-rays: analysis using a convolution/superposition method *Phys. Med. Biol.* **35** 1533–49

Mijnheer B J, Battermann J J and Wambersie A 1987 What degree of accuracy is required and can be achieved in photon and neutron therapy? *Radiother. Oncol.* **8** 237–52

Mohan R and Chui C S 1985 Validity of the concept of separating primary and scatter dose *Med. Phys.* **12** 726–30

——1987 Use of fast Fourier transforms in calculating dose distributions for irregularly shaped fields for three-dimensional treatment planning *Med. Phys.* **14** 70–7

Mohan R, Chui C and Lidofsky L 1985 Energy and angular distributions of photons from medical linear accelerators *Med. Phys.* **12** 592–7

——1986 Differential pencil beam dose computation model for photons *Med. Phys.* **13** 64–73

Mohan R, Chui C, Miller D and Laughlin J S 1981 Use of computerized tomography in dose calculations for radiation treatment planning *J. Comput. Tomogr.* **5** 273–82

Mohan R, Wu Q, Wang X and Stein J 1996 Intensity modulation optimization, lateral transport of radiation, and margins *Med. Phys.* **23** 2011–21

Murray D C, Hoban P W, Metcalfe P E and Round W H 1989 3-D superposition for radiotherapy treatment planning using fast Fourier transforms *Australas. Phys. Eng. Sci. Med.* **12** 128–37

Murray D C, Hoban P W, Round W H, Graham I D and Metcalfe P E 1991 Superposition on a multicomputer system *Med. Phys.* **18** 468–73

Nelson W R, Hirayama H and Rogers D W O 1985 The EGS4 code system *Stanford Linear Accelerator Report* 265

NEMA 1998 *Digital Imaging and Communication in Medicine (DICOM)* PS 3.1-3.14 (National Electrical Manufacturers Association)

Neuenschwander H, Mackie T R and Reckwerdt P J 1995 MMC—a high-performance Monte Carlo code for electron beam treatment planning *Phys. Med. Biol.* **40** 543–74

Niemierko A and Goitein M 1990 Random sampling for evaluating treatment plans *Med. Phys.* **17** 753–62

Nigg D W, Randolph P D and Wheeler F J 1991 Demonstration of three-dimensional deterministic radiation transport theory dose distribution analysis for boron neutron capture therapy *Med. Phys.* **18** 43–53

Nilsson B 1985 Electron contamination from different materials in high energy photon beams *Phys. Med. Biol.* **30** 139–51

Nilsson B and Brahme A 1979 Absorbed dose from secondary electrons in high energy photon beams *Phys. Med. Biol.* **24** 901–12

——1981 Contamination of high-energy photon beams by scattered photons *Strahlentherapie* **157** 181–6

——1986 Electron contamination from photon beam collimators *Radiother. Oncol.* **5** 235–44

Nilsson M and Knöös T 1992 Application of the Fano theorem in inhomogeneous media using a convolution algorithm *Phys. Med. Biol.* **37** 69–83

Nisbet A, Weatherburn H, Fenwick J D and McVey G 1998 Spectral reconstruction of clinical megavoltage photon beams and the implications of spectral determination on the dosimetry of such beams *Phys. Med. Biol.* **43** 1507–21

Nizin P S 1993 Electronic equilibrium and primary dose in collimated photon beams *Med. Phys.* **20** 1721–9

Nordell B and Brahme A 1984 Angular distribution and yield from bremsstrahlung targets *Phys. Med. Biol.* **29** 797–810

O'Connor J E 1957 The variation of scattered x-rays with density in an irradiated body *Phys. Med. Biol.* **1** 352–69

O'Connor J E and Malone D E 1989 A cobalt-60 primary dose spread array derived from measurements *Phys. Med. Biol.* **34** 1029–42

Ostapiak O Z, Zhu Y and Van Dyk J 1997 Refinements of the finite-size pencil beam model of three-dimensional photon dose calculation *Med. Phys.* **24** 743–50

Overgaard J and Bartelink H 1995 About tolerance and quality. An important notice to all radiation oncologists *Radiother. Oncol.* **35** 1–3

Papanikolaou N, Mackie T R, Meger-Wells C, Gehring M and Reckwerdt P 1993 Investigation of the convolution method for polyenergetic spectra *Med. Phys.* **20** 1327–36

Patomaki L K 1968 The equivalent field principle and its use in beam therapy dose calculations *Br. J. Radiol.* **41** 381–3

Petti P L, Rice R K, Mijnheer B J, Chin L M and Bjärngard B E 1987 A heterogeneity model for photon beams incorporating electron transport *Med. Phys.* **14** 349–54

Piermattei A, Arcovito G, Azario L, Bacci C, Bianciardi L, De Sapio E and Giacco C 1990 A study of quality of bremsstrahlung spectra reconstructed from transmission measurements *Med. Phys.* **17** 227–33

Purdy J A 1992 Photon dose calculations for three-dimensional radiation treatment planning *Semin. Radiat. Oncol.* **2** 235–45

Purdy J A and Prasad S C 1983 Current methods and algorithms in radiation absorbed dose calculation and the role of computed tomography: a review *Computed Tomography in Radiation Therapy* ed C C Ling, C C Rogers and R J Morton (New York: Raven Press) pp 187–97

Purdy J A, Wong J W, Harms W B, Emami B and Matthews J W 1987 State of the art of high energy photon treatment planning *Front. Radiat. Therapy Oncol.* **21** 4–24

Rathee S, McClean B A and Field C 1993 An improved method for rebinning kernels from cylindrical to Cartesian coordinates. *Med. Phys.* **20** 1343–51

Reckwerdt P J and Mackie T R 1992 Superposition/convolution speed improvements using run-length raytracing (AAPM abstract) *Med. Phys.* **19** 784

Redpath A T 1995 A beam model for 3-dimensional radiotherapy planning *Br. J. Radiol.* **68** 1356–63

Redpath A T and Thwaites D I 1991 A 3-dimensional scatter correction algorithm for photon beams *Phys. Med. Biol.* **36** 779–98

Roesch W M C 1958 Dose for nonelectronic equilibrium conditions *Radiat. Res.* **9** 399–410

Rogers D W O and Bielajew A F 1990 Monte Carlo techniques of electron and photon transport for radiation *The Dosimetry of Ionizing Radiation* vol 3, ed K R Kase, B Bjärngard and F H Attix (New York: Academic) pp 427–539

Rogers D W O, Faddegon B A, Ding G X, Ma C M, We J and Mackie T R 1995 BEAM: a Monte Carlo code to simulate radiotherapy treatment units *Med. Phys.* **22** 503–24

Rossi H H and Roesch W C 1962 Field equations in dosimetry *Radiat. Res.* **16** 783–95

Sätherberg A, Karlsson M and Karlsson M 1996 Theoretical and experimental determination of phantom scatter factors for photon fields with different radial energy variation *Phys. Med. Biol.* **41** 2687–94

Sauer O A 1994 Dosisverteilungen an Material-Grenzflächen bei energiereichen Röntgenstrahlen *PhD Thesis* University of Julius-Maximilians Würzburg

——1995 Calculation of dose distributions in the vicinity of high-Z interfaces for photon beams *Med. Phys.* **22** 1685–90

Sauer O and Neumann M 1990 Reconstruction of high-energy bremsstrahlung spectra by numerical analysis of depth-dose data *Radiother. Oncol.* **18** 39–47

Saxner M and Ahnesjö A 1998 Implementation of the collapsed cone method for clinical beam qualities *Med. Phys.* **25** A185

Saxner M, Löfgren A and Ahnesjö A 1997 Integration of head scatter fluence calculations in treatment planning *Int. Conf. on the Use of Computers in Radiation Therapy, XII ICCR (Salt Lake City, Utah, USA)* ed D D Leavitt and G Starkschall (Madison, WI: Medical Physics Publishing) pp 213–15

Schad L R, Gademann G, Knopp M, Zabel H J, Schlegel W and Lorenz W J 1992 Radiotherapy treatment planning of basal meningiomas: improved tumor localization by correlation of CT and MR imaging data *Radiother. Oncol.* **25** 56–62

Schoknecht G 1971 Die Beschreibung von Strahlenfeldern durch Separierung von Primär- und Streustrahlung IV. Berechnung von Streuverteilungen für parallele Photonenstrahlenfelder *Strahlentherapie* **141** 326–31

Shapiro A, Lin B I, Windham J P and Kereiakes J G 1976 Transport calculations of gamma ray flux density and dose rate about implantable californium-252 sources *Phys. Med. Biol.* **21** 509–23

Sharpe M B and Battista J J 1993 Dose calculations using convolution and superposition principles: the orientation of dose spread kernels in divergent x-ray beams *Med. Phys.* **20** 1685–94

Sharpe M B, Jaffray D A, Battista J J and Munro P 1995 Extrafocal radiation: a unified approach to the prediction of beam penumbra and output factors for megavoltage x-ray beams *Med. Phys.* **22** 2065–74

Siddon R L 1985 Fast calculation of the exact radiological path for a three-dimensional CT array *Med. Phys.* **12** 252–5

Siddon R L, Dewyngaert J K and Bjärngard B E 1985 Scatter integration with right triangular fields *Med. Phys.* **12** 229–31

Silver M D 1994 Target self-attenuation extension to the Desobry and Boyer thick-target bremsstrahlung spectrum *Med. Phys.* **21** 577–9

Sjögren R and Karlsson M 1996 Electron contamination in clinical high energy photon beams *Med. Phys.* **23** 1873–81

Söderström S, Gustafsson A and Brahme A 1993 The clinical value of different treatment objectives and degrees of freedom in radiation therapy optimization *Radiother. Oncol.* **29** 148–63

Sontag M R 1979 Photon beam dose calculations in regions of tissue heterogeneity using computed tomography *PhD Thesis* University of Toronto

Sontag M R and Cunningham J R 1977 Corrections to absorbed dose calculations for tissue inhomogeneities *Med. Phys.* **4** 431–6

——1978a Clinical application of a CT based treatment planning system *Comput. Tomogr.* **2** 117–30

——1978b The equivalent tissue-air ratio method for making absorbed dose calculations in a heterogeneous medium *Radiology* **129** 787–94

Sontag M R and Ray S K 1995 Determination of differential scatter-air ratios (dSAR) for three-dimensional scatter integration *Med. Phys.* **22** 775–80

Sterling T D, Perry H and Katz L 1964 Automation of radiation treatment planning IV. Derivation of a mathematical expression for the per cent depth dose surface of cobalt 60 beams and visualisation of multiple field dose distributions *Br. J. Radiol.* **37** 544–50

Storchi P and van Gasteren J J M 1996 A table of phantom scatter factors of photon beams as a function of the quality index and field size *Phys. Med. Biol.* **41** 563–71

Storchi P and Woudstra E 1996 Calculation of the absorbed dose distribution due to irregularly shaped photon beams using pencil beam kernels derived form basic beam data *Phys. Med. Biol.* **41** 637–56

Storchi P, Woudstra E, Verlinde P, Johansson K-A and Samuelsson A 1998 Calculation of absorbed dose distributions from dynamic wedges *Phys. Med. Biol.* **43** 1497–506

Sundblom I 1965 Dose planning for irradiation of thorax with ^{60}Co in fixed-beam teletherapy *Acta Radiol.* **3** 342–52

Svensson H and Brahme A 1986 Recent advances in electron and photon dosimetry *Radiation Dosimetry, Physical and Biological Aspects* ed C G Orton (New York: Plenum) pp 87–170

Svensson R and Brahme A 1996 Effective source size, yield and beam profile from multi-layered bremsstrahlung targets *Phys. Med. Biol.* **41** 1353–79

Svensson R, Källman P and Brahme A 1994 An analytical solution for the dynamic control of multileaf collimators *Phys. Med. Biol.* **39** 37–61

Swindell W, Simpson R G, Oleson J R, Chen C-T and Grubbs F A 1983 Computed tomography with a linear accelerator with radiotherapy applications *Med. Phys.* **10** 416–20

Tailor R C, Tello V M, Schroy C B, Vossler M and Hanson W F 1998 A generic off-axis energy correction for linac photon beam dosimetry *Med. Phys.* **25** 662–7

Tatcher M and Bjärngard B E 1993 Equivalent squares of irregular photon fields *Med. Phys.* **20** 1229–32

Thomas S J 1991 A modified power-law formula for inhomogeneity corrections in beams of high-energy x-rays *Med. Phys.* **18** 719–23

Treuer H, Boesecke R, Hartmann G H, Schlegel W and Lorenz W J 1987 Dosimetrische Bestimmung der Primärfluenz und der Fokusgrösse eines 15-MeV-Linearbeschleunigers. *Med. Physik* 375–80

Ulmer W 1982 On the application of stochastic partition functions for the computation of lateral profiles and depth doses in radiotherapy *Strahlentherapie* **158** 305–11

Uwamino Y, Nakamura T, Ohkubo T and Hara A 1986 Measurement and calculation of neutron leakage from a medical electron accelerator *Med. Phys.* **13** 374–84

van de Geijn J 1987 The extended net fractional depth dose: correction for inhomogeneities, including effects of electron transport in photon beam dose calculation *Med. Phys.* **14** 84–92

Van Dyk J, Barnett R B, Cygler J E and Shragge P C 1993 Commissioning and quality assurance of treatment planning computers *Int. J. Radiat. Oncol. Biol. Phys.* **26** 261–73

van Gasteren J J M, Heukelom S, van Kleffens H J, van der Laarse R, Venselaar J L M and Westermann C F 1991 The determination of phantom and collimator scatter components of the output of megavoltage photon beams: measurement of the collimator scatter part with a beam-coaxial narrow cylindrical phantom. *Radiother. Oncol.* **20** 250–7

van Santvoort J P C and Heijmen B J M 1996 Dynamic multileaf collimation without 'tongue-and-groove' underdosage effects *Phys. Med. Biol.* **41** 2091–105

van't Veld A A 1997 Analysis of accuracy in dose and position in calculations of a treatment planning system for blocked photon fields *Radiother. Oncol.* **45** 245–51

van't Veld A A and Bruinvis I A 1995 Influence of shape on the accuracy of grid-based volume computations *Med. Phys.* **22** 1377–85

Wagner J C, Redmond II E L, Palmtag S P and Hendricks J S 1994 MCNP: multigroup/adjoint capabilities *Report* LA-12704 (Los Alamos National Laboratory)

Wang L, Chui C-S and Lovelock M 1998 A patient-specific Monte Carlo dose-calculation method for photons beams *Med. Phys.* **25** 867–78

Wang L, Zhu Y and Jette D 1995 Analytic modeling of the primary x-ray dose deposition kernels (abstract) *Med. Phys.* **22** 977

Webb S 1993 *The Physics of Three-Dimensional Radiation Therapy. Conformal Radiotherapy, Radiosurgery and Treatment Planning (Medical Science Series)* (Bristol: Institute of Physics Publishing)

——1997 *The Physics of Conformal Radiotherapy Advances in Technology (Medical Science Series)* (Bristol: Institute of Physics Publishing)

——1998a Configuration options for intensity-modulated radiation therapy using multiple static fields shaped by a multileaf collimator *Phys. Med. Biol.* **43** 241–60

——1998b Configuration options for intensity-modulated radiation therapy using multiple static fields shaped by a multileaf collimator. II: Constraints and limitations on 2D modulation. *Phys. Med. Biol.* **43** 1481–95

Webb S and Fox R A 1980 Verification by Monte Carlo methods of a power law tissue-air ratio algorithm for inhomogeneity corrections in photon beam dose calculations *Phys. Med. Biol.* **25** 225–40

Weber L, Ahnesjö A, Nilsson P, Saxner M and Knöös T 1996 Verification and implementation of dynamic wedge calculations in a treatment planning system based on a dose-to-energy-fluence formalism *Med. Phys.* **23** 307–16

Weber L, Nilsson P and Ahnesjö A 1997 Build-up cap materials for mesurement of photon head-scatter factors *Phys. Med. Biol.* **42** 1875–86

Wong E, Van Dyk J and Zhu Y 1997 Lateral electron transport in FFT photon dose calculations *Med. Phys.* **24** 1992–2000

Wong E, Zhu Y and Van Dyk J 1996 Theoretical developments on fast Fourier transform convolution dose calculations in inhomogeneous media *Med. Phys.* **23** 1511–21

Wong J W and Henkelman R M 1982 Reconsideration of the power-law (Batho) equation for inhomogeneity corrections *Med. Phys.* **9** 521–30

——1983 A new approach to CT pixel-based photon dose calculations in heterogeneous media *Med. Phys.* **10** 199–208

Wong J W, Henkelman R M, Andrew J W, Van Dyk J and Johns H E 1981a Effect of small inhomogeneities on dose in a cobalt-60 beam *Med. Phys.* **8** 783–91

Wong J W, Henkelman R M, Fenster A and Johns H E 1981b Second scatter contribution to dose in a cobalt-60 beam *Med. Phys.* **8** 775–82

Wong J W and Purdy J A 1987 Basis of recent methods of photon dose calculations *9th Int. Conf. on The Use of Computers in Radiation Therapy (Scheveningen, The Netherlands)* ed I A D Bruinvis, P H van der Giessen, H J van Kleffens and F H Wittkampher (Amsterdam: Elsevier) pp 319–22

——1990 On methods of inhomogeneity corrections for photon transport. *Med. Phys.* **17** 807–14

——1992 Review of methods of inhomogeneity corrections *Advances in Radiation Oncology Physics: Dosimetry, Treatment Planning and Brachytherapy* (New York: American Institute of Physics) pp 887–99

Wong J W, Slessinger E D, Hermes R E, Offutt C J, Roy T and Vannier M W 1990 Portal dose images I: Quantitative treatment plan verification *Int. J. Radiat. Oncol. Biol. Phys.* **18** 1455–63

Wong J W, Slessinger E D, Rosenberger F U, Krippner K and Purdy J A 1984 The delta volume method for 3-dimensional photon dose calculations *Int. Conf. on the Use of Computers in Radiation Therapy, VIII ICCR (Toronto, Canada)* (Silver Spring, MD: IEEE Computer Society Press) pp 26–30

Woo M K 1994 Analysis of photon beam exit dose using photon point kernels *Phys. Med. Biol.* **39** 687–702

Woo M K and Cunningham J R 1990 The validity of the density scaling method in primary electron transport for photon and electron beams *Med. Phys.* **17** 187–94

Woo M K, Cunningham J R and Jezioranski J J 1990 Extending the concept of primary and scatter separation to the condition of electronic disequilibrium *Med. Phys.* **17** 588–95

Worthley B 1966 Equivalent square of rectangular fields (letter) *Br. J. Radiol.* **39** 559

Wrede D E 1972 Central axis tissue–air ratios as a function of area-perimeter at depth and their applicability to irregularly shaped fields *Phys. Med. Biol.* **17** 548–54

Yan D, Ziaja E, Jaffray D, Wong J, Brabbins D, Vicini F and Martinez A 1998 The use of adaptive radiation therapy to reduce setup error: a prospective clinical study *Int. J. Radiat. Oncol. Biol. Phys.* **41** 715–20

Ying X, Geer L Y and Wong J W 1990 Portal dose images II: Patient dose estimation *Int. J. Radiat. Oncol. Biol. Phys.* **18** 1465–75

Yu C X, Mackie T R and Wong J W 1995 Photon dose calculation incorporating explicit electron transport *Med. Phys.* **22** 1157–65

Yu C X and Wong J W 1993 Implementation of the ETAR method for 3D inhomogeneity correction using FFT *Med. Phys.* **20** 627–32

Yu M K, Sloboda R S and Mansour F 1996 Measurement of photon beam backscatter from collimators to the beam monitor chamber using target-current-pulse-counting and telescope techniques *Phys. Med. Biol.* **41** 1107–17

Yu M K, Sloboda R S and Murray B 1997 Linear accelerator photon beam quality at off-axis points *Med. Phys.* **24** 233–9

Zefkili S, Kappas C and Rosenwald J C 1994 On-axis and off-axis primary dose component in high energy photon beams *Med. Phys.* **21** 799–808

Zhu T C and Bjärngard B E 1995 The fraction of photons undergoing head scatter in x-ray beams *Phys. Med. Biol.* **40** 1127–34

Zhu T C and Palta J R 1998 Electron contamination in 8 and 18 MV photon beams *Med. Phys.* **25** 12–19

Zhu Y and Boyer A 1990 X-ray dose computations in heterogeneous media using 3-dimensional FFT convolution *Phys. Med. Biol.* **35** 351–68

Zhu Y and Van Dyk J 1995 Accuracy requirements of the primary x-ray spectrum in dose calculations using FFT convolution techniques *Med. Phys.* **22** 421–6